



Lawrence Berkeley Laboratory

UNIVERSITY OF CALIFORNIA

EARTH SCIENCES DIVISION

A STUDY OF ATES THERMAL BEHAVIOR USING
A STEADY FLOW MODEL

Christine Doughty, Göran Hellström,
Chin Fu Tsang, and Johan Claesson

January 1981

TWO-WEEK LOAN COPY

*This is a Library Circulating Copy
which may be borrowed for two weeks.
For a personal retention copy, call
Tech. Info. Division, Ext. 6782*



LBL Library

DISCLAIMER

This document was prepared as an account of work sponsored by the United States Government. While this document is believed to contain correct information, neither the United States Government nor any agency thereof, nor the Regents of the University of California, nor any of their employees, makes any warranty, express or implied, or assumes any legal responsibility for the accuracy, completeness, or usefulness of any information, apparatus, product, or process disclosed, or represents that its use would not infringe privately owned rights. Reference herein to any specific commercial product, process, or service by its trade name, trademark, manufacturer, or otherwise, does not necessarily constitute or imply its endorsement, recommendation, or favoring by the United States Government or any agency thereof, or the Regents of the University of California. The views and opinions of authors expressed herein do not necessarily state or reflect those of the United States Government or any agency thereof or the Regents of the University of California.

A STUDY OF ATES THERMAL BEHAVIOR
USING A STEADY FLOW MODEL

Christine Doughty*, Göran Hellström^{†*}, Chin Fu Tsang*, and Johan Claesson[†]

*Earth Sciences Division
Lawrence Berkeley Laboratory
University of California
Berkeley, California 94720

[†]Department of Mathematical Physics
Lund Institute of Technology
Lund, Sweden

January 1981

This work was supported by the Assistant Secretary of Conservation and Solar Energy, Office of Advanced Conservation Technology, Division of Thermal and Mechanical Storage Systems of the U. S. Department of Energy under contract W-7405-ENG-48. This report represents work performed within the Seasonal Thermal Energy Storage program managed by Pacific Northwest Laboratory. On the Swedish side, the work has been supported by the National Swedish Board for Energy Source Development (NE).

I. INTRODUCTION

The concept of heat storage in an aquifer has attracted increasing interest during the last five years (Lawrence Berkeley Laboratory, 1978; Tsang, Hopkins and Hellström, 1980). The basic idea is to inject hot water into an aquifer during periods of low energy demand, and then, when energy demand is high, to extract the water and use the heat. The energy supply may come from a variety of sources, such as solar energy, industrial waste heat, or power plant cogeneration. An aquifer naturally provides a large volume of water as the storage medium, at a relatively low cost. Water is extracted from the aquifer through a supply well, and, after being heated, is injected into a storage well in the same aquifer. After the hot water has been produced from the storage well and the heat used, the water is reinjected into the supply well, thereby creating a closed system with little net groundwater consumption. Aquifer thermal energy storage (ATES) is considered to be one of the most promising and cost effective alternatives for low temperature heat storage on a large scale. Numerous theoretical investigations estimate that as much as 80-90% of the injected energy may be recovered during a seasonal ATES cycle (Tsang, Lippmann, Goranson and Witherspoon, 1977; Fabris, Gringarten, Landel, Noyer and Sauty, 1977). Recently Sauty et al. (1980) have studied the thermal behavior of a simplified single well ATES system in terms of a set of dimensionless groups.

A few field experiments of heat storage in either confined (Molz et al., 1981; Yokoyama et al., 1978) or unconfined aquifers (Mathey, 1977; Fabris and Gringarten, 1977; Iris, 1979; Reddell, Davison and Harris, 1978) have been completed. Most of these aquifers are rather shallow and of high permeability. Experiments involving the storage of cold water for air conditioning have also been done (Yokoyama et al., 1978; Reddell et al., 1978). The highest injection temperature (55°C) and largest injection volume (55,000 m³)

experiment to date has been carried out by Auburn University (Alabama, USA) where two consecutive six month cycles yielded recoveries of 66 and 76% of the injected energy. These are promising values considering the relatively small injection volume. However, many problems, both theoretical and practical, need to be solved in order to make it possible to assess the feasibility of hot water storage in a specific aquifer at a given site. These problems relate to legal and environmental issues, water chemistry, soil mechanics, and thermo-hydraulics.

This study considers the thermal behavior around a storage well in the case when buoyancy effects can be neglected. A dimensionless formulation of the energy transport equations for the aquifer system is presented, and the key dimensionless parameters are discussed. A numerical model using a steady flow field is used to simulate heat transport in the aquifer and confining layers around the injection/production well during the ATES cycle. The key parameters are varied in order to understand their influence on the percent of the injected energy that can be recovered, and the temperature of the extracted water. The results are presented graphically. Finally, some comparisons with field experiments are given to illustrate the use of the dimensionless groups and graphs. This study follows similar lines to that of Sauty et al.(1980), but considers a more general system, and extends the results in different areas.

II. Conceptual Model

II.1 Definitions

The ATES system considered consists of a single injection/production well that fully penetrates an infinite, horizontal aquifer of uniform thickness, H . Results are also applicable for a multiple well system where well spacing is large enough so that the thermal behavior around the storage well is not significantly affected by neighboring wells.

This has been studied to some extent by Tsang, Buscheck, Mangold and Lippmann (1978). Under the single well idealization, there is radial symmetry with respect to the well. Furthermore the aquifer is assumed to be homogeneous with thermal conductivity, λ_a , heat capacity per unit volume, C_a , and dispersive lengths $d_{||}$ and d_{\perp} (see list of nomenclature for definitions of all symbols). It is bounded above and below by impermeable confining layers which may be of arbitrary thickness and composition. This study considers a system with a caprock of thickness D and an infinitely thick bedrock. Both caprock and bedrock are homogeneous and have thermal conductivity λ_c and heat capacity per unit volume C_c . The heat capacity per unit volume of water is C_w . All material properties are assumed to be temperature independent.

The length of the ATES cycle is t_c . The duration of injection, storage, production, and rest periods are t_i , t_s , t_p , and t_r respectively. The magnitude of the volumetric fluid flow rate, Q , is kept constant during injection and production periods, and the injected and produced volumes are taken to be equal, that is $Q_i t_i = Q_p t_p \equiv V_w$.

In a hypothetical aquifer storage system with no heat conduction, the energy transport would only take place by convection. At the end of the injection period a cylindrical region around the injection well would have constant temperature T_1 , while the rest of the system could remain at T_0 . This region at T_1 is called the thermal volume, V , it is defined by $V = (C_w/C_a)V_w$. The thermal volume may also be written as $V = \pi R^2 H$, where R is the thermal radius. Hence, R is defined as

$$R = \sqrt{\frac{V}{\pi H}} = \sqrt{\frac{V C_w}{C_a \pi H}} \quad (1)$$

An essential result of our calculations is the time-varying temperature, T_p , of the water extracted from the aquifer during the production period.

The energy recovery factor, ϵ , for each cycle is defined as the ratio between the produced and injected energy when equal volumes of water are injected into and produced from the aquifer. The energy content of the water is defined using the original ambient temperature of the aquifer, T_0 , as a reference. The temperature of the injected water is T_1 . The recovery factor, ϵ , is:

$$\epsilon = \frac{\int_{t_i + t_s}^{t_i + t_s + t_p} (C_w T_p - C_w T_0) Q_p dt}{\int_0^{t_i} (C_w T_1 - C_w T_0) Q_i dt} \quad (2)$$

This expression can be written as:

$$\epsilon = \frac{\bar{T}_p - T_0}{T_1 - T_0} \quad (3)$$

where \bar{T}_p denotes the average temperature of the produced water during the production period. A dimensionless temperature, T' , is defined as:

$$T' = \frac{T - T_0}{T_1 - T_0} \quad (4)$$

The expression for the recovery factor (2) then becomes:

$$\epsilon = \bar{T}'_p \quad (5)$$

where \bar{T}'_p is the average dimensionless temperature of the produced water.

In most applications there will be a cut-off temperature, below which energy is not usable, which will probably be higher than T_0 . The recovery factor, ϵ_{ref} , calculated with respect to a dimensionless reference (cut-off) temperature, T'_{ref} , is:

$$\epsilon_{ref} = \frac{(\epsilon - T'_{ref})}{(1 - T'_{ref})} \quad (6)$$

If the temperature of the produced water falls below the reference temperature during a part of the production period, equation 6 is not correct, because the production will stop when the reference temperature is reached, not when the produced volume is equal to the injected volume. In such a case equation 2, with T_0 replaced by T_{ref} , may be used to calculate the percent of energy above T_{ref} that is recovered. However this percent is not a recovery factor as we have defined it, because the produced and injected volumes are not equal.

Throughout this paper the injected energy is referred to as heat, however, all the results discussed also apply to chilled water storage.

The influence of regional ground water flow on the thermal recovery of the storage system has not been studied. However, if this influence may become large, the storage region in the aquifer will have to be protected, for example by using boundary wells (Tsang and Witherspoon, 1975; Whitehead and Langhete, 1978).

II.2 Buoyancy Flow

In this study the only fluid flow is a steady radial flow, and fluid density is assumed to be constant. Hence, buoyancy flow induced by the density difference between injected warm water and the cold water in the aquifer is neglected. This is somewhat justified for low permeability aquifers, cases with small temperature differences between injected and original waters, or short cycle lengths. Under these conditions, buoyancy flow can be neglected. Additionally, for geometries in which the thermal radius is much greater than the aquifer thickness, a moderate tilting of the thermal front caused by buoyancy flow may have only a small effect on the overall thermal behavior of the system. A theory proposed by Hellström, Tsang, and Claesson (1979) gives a formula for the characteristic time constant, t_0 , for the buoyancy tilting

rate of the hot-cold water interface. This formula, which is given in Appendix A, may be used to determine cases where buoyancy flow may be neglected. On the other hand, the conclusions presented in this paper may still be applicable in a relative sense, even in cases where buoyancy flow is significant.

II.3 Dimensionless Formulation and Definition of Dimensionless Parameters

The thermal behavior of the aquifer storage system may be expressed in dimensionless form. We assume, as a reasonable approximation to the seasonal variation of supply and demand of energy, that the injection, storage, production, and rest periods are of equal duration so that $t_i = t_s = t_p = t_r = t_c/4$. In this section we shall also assume the caprock to be of infinite thickness and the dispersive lengths to be zero. The effects of unequal length periods, a finite caprock and velocity-dependent dispersion will be treated as special cases (Sections III.2.1 - III.2.3) and are not considered in the following formulation. The system is symmetric about the midplane of the aquifer, $z = 0$. Hence, only the region $z \geq 0$ need be considered.

The temperature field in the confining layers is governed by the ordinary heat conduction equation, namely:

$$\lambda_c \frac{\delta^2 T}{\delta \rho^2} + \lambda_c \frac{1}{\rho} \frac{\delta T}{\delta \rho} + \lambda_c \frac{\delta^2 T}{\delta z^2} = C_c \frac{\delta T}{\delta t} \quad z > \frac{H}{2} \quad (7)$$

Assuming an incompressible radial flow in the aquifer, the heat balance equation in the aquifer may be written as:

$$\lambda_a \frac{\delta^2 T}{\delta \rho^2} + \lambda_a \frac{1}{\rho} \frac{\delta T}{\delta \rho} + \lambda_a \frac{\delta^2 T}{\delta z^2} - \frac{C_w Q}{2\pi H} \cdot \frac{1}{\rho} \frac{\delta T}{\delta \rho} = C_a \frac{\delta T}{\delta t} \quad z < \frac{H}{2} \quad (8)$$

The last term on the left side represents the convective heat transport in the aquifer due to pumping at the well. Temperature and heat flow must be continuous at the interface between aquifer and confining layer, i.e.:

$$T \Big|_{z = \frac{H}{2} + 0} = T \Big|_{z = \frac{H}{2} - 0} \quad (9)$$

and:

$$\lambda_c \frac{\delta T}{\delta z} \Big|_{z = \frac{H}{2} + 0} = \lambda_a \frac{\delta T}{\delta z} \Big|_{z = \frac{H}{2} - 0} \quad (10)$$

Let us choose the following dimensionless parameters:

$$t' = \frac{t}{t_i} \quad \rho' = \frac{\rho}{L} \quad z' = \frac{z}{L} \quad (11)$$

where

$$L = \sqrt{\frac{\lambda_a}{\lambda_c} \frac{\lambda_c t_i}{C_c}}$$

Further, if we define

$$Pe = \frac{QC_w}{2\pi\lambda_a H} \quad (12)$$

as the Peclet number, then using the dimensionless temperature T' (4), the equations 7, 8, 9, and 10 become:

$$\frac{\delta^2 T'}{\delta \rho'^2} + \frac{1}{\rho'} \frac{\delta T'}{\delta \rho'} + \frac{\delta^2 T'}{\delta z'^2} = \frac{\lambda_a}{\lambda_c} \frac{\delta T'}{\delta t'} \quad z' > \frac{H}{2L} \quad (13)$$

$$\frac{\delta^2 T'}{\delta \rho'^2} + \frac{1}{\rho'} \frac{\delta T'}{\delta \rho'} + \frac{\delta^2 T'}{\delta z'^2} - Pe \frac{1}{\rho'} \frac{\delta T'}{\delta \rho'} = \frac{C_a}{C_c} \frac{\delta T'}{\delta t'} \quad z' < \frac{H}{2L} \quad (14)$$

$$T' \Big|_{z' = \frac{H}{2L} + 0} = T' \Big|_{z' = \frac{H}{2L} - 0} \quad (15)$$

$$\frac{\delta T'}{\delta z'} \Big|_{z' = \frac{H}{2L} + 0} = \frac{\lambda_a}{\lambda_c} \frac{\delta T'}{\delta z'} \Big|_{z' = \frac{H}{2L} - 0} \quad (16)$$

Based on the form of these equations, the temperature at any point may now be written as:

$$T' = T' \left(\rho', z', t', Pe, \frac{C_a}{C_c}, \frac{\lambda_a}{\lambda_c}, \frac{H}{2L} \right) \quad (17)$$

The temperature, T'_p , of water produced from the aquifer will be an average of the vertical temperature distribution in the aquifer at the well, which is located at $\rho' = 0$. It is given by:

$$T'_p = \frac{L}{H} \int_{-H/2L}^{H/2L} T \left(0, z', t', Pe, \frac{C_a}{C_c}, \frac{\lambda_a}{\lambda_c}, \frac{H}{2L} \right) dz' \quad (18)$$

The factor $H/2L$ can be rewritten in terms of C_a/C_c , λ_a/λ_c , and a parameter, Λ , introduced by Fabris et al. (1977), which is defined as:

$$\Lambda = \frac{C_a^2 H^2}{C_c \lambda_c t_i} \quad (19)$$

This implies that the temperature of the produced water is:

$$T'_p = T'_p \left(t', Pe, \frac{C_a}{C_c}, \frac{\lambda_a}{\lambda_c}, \Lambda \right) \quad (20)$$

The recovery factor (5) is the average temperature of the produced water during the production period. The dimensionless groups controlling the recovery factor are summarized as follows:

$$\circ \quad Pe = \frac{QC_w}{2\pi\lambda_a H} = \frac{C_a R^2}{2\lambda_a t_i} \quad (21)$$

$$\circ \quad \Lambda = \frac{C_a^2 H^2}{C_c \lambda_c t_i}$$

$$\circ \quad \frac{\lambda_a}{\lambda_c}$$

$$\circ \quad \frac{C_a}{C_c}$$

o The number of cycles.

II.4 Steady Flow Model

Detailed numerical models which solve the coupled mass and energy transfer equations of fluid flow in a porous medium have been successfully used to match analytical results (Tsang et al., 1977) as well as field data (Tsang, Buscheck and Doughty, 1980; Papadopoulos and Larson, 1978) for ATES systems. Generally these models are expensive and time consuming to run. For the purpose of gaining a better understanding of the processes controlling heat loss in an ATES cycle, it is often desirable to do a series of simulations in which different parameters are systematically varied. To this end, the present study uses a simplified, but fast, numerical model of mass and energy transfer in an aquifer system. This model, the steady flow model (SFM) was developed by Lund University (Hellström and Claesson, 1978) and modified at Lawrence Berkeley Laboratory for our present study.

Rather than solving the mass transfer equation to obtain a fluid flow field as a function of time, a steady horizontal flow field is prescribed in the aquifer, leading to an energy transfer equation given by equation 8.

In general, the numerical simulation of a combined convection and conduction equation such as equation 8 introduces a mesh dependent numerical dispersion, which causes spurious thermal front smearing. The SFM avoids this effect by simulating the flow field in a special way described below. In contrast, when the coupled equations for mass and heat transport are solved with temperature dependent properties, as in most detailed numerical models, it is not possible to avoid a certain amount of numerical dispersion.

The flow field is simulated in the following way: a mesh is constructed in which all the elements of a horizontal row have equal volumes. Due to the cylindrical symmetry, the radial dimension of the elements decreases as the radial distance from the well to the element increases, as shown in Figure 1. The thermal front radius, R , at the end of the injection period, the number of the number of mesh elements, M , in each row between $\rho = 0$ and R , and the duration of the injection period, t_i , are given as input to the program. The length of the m th element is $R_{m+1} - R_m$, where $R_m = \sqrt{(m-1)/M} R$. The volume of the m th element is proportional to $R_{m+1}^2 - R_m^2$, which is independent of m . During the injection period, whenever time t is equal to t_i/M , $2t_i/M$, $3t_i/M \dots t_i$, the temperature distribution in the aquifer is translated horizontally one element away from the well and the user specified injection temperature, T_1 , is assigned to the first element in each row. This translation every timestep, t_i/M , simulates a constant volumetric fluid flow rate at the well:

$$Q_i = \frac{C_a \pi R_H^2}{C_w t_i} \left(\frac{m}{s} \right)^3 \quad (22)$$

and a horizontal Darcy velocity:

$$v(\rho) = \frac{Q_i}{2\pi H \rho} \left(\frac{m}{s} \right) \quad (23)$$

at radius ρ in the aquifer. When $t = t_i$, the temperature field has been translated M times and the thermal front radius is R .

Heat transfer by convection is accounted for by translation of the aquifer temperature field every time step t_1/M . Heat transfer by conduction is described by the ordinary heat equation:

$$C \frac{\delta T}{\delta t} = \nabla (\lambda \nabla T) = - \nabla \cdot \underline{q} \quad (24)$$

where \underline{q} is the heat flow per unit area. Equation 24 is solved numerically for each element in the mesh during every timestep Δt . For the (m,n) th element in the mesh it is written:

$$\int_{V_{m,n}} C_{m,n} \frac{\delta T}{\delta t} dV = - \int_{V_{m,n}} \nabla \cdot \underline{q} dV = - \int_{A_{m,n}} \underline{q} \cdot \hat{n} dA \quad (25)$$

where the righthand side describes the heat transfer to all neighboring elements.

Using the explicit finite difference approximation equation 25 becomes:

$$C_{m,n} V_{m,n} \frac{(T_{m,n}(t + \Delta t) - T_{m,n}(t))}{\Delta t} = \quad (26)$$

$$\begin{aligned} & q_{\rho}^{m,n} 2\pi R_m (z_{n+1} - z_n) - q_{\rho}^{m+1,n} 2\pi R_{m+1} (z_{n+1} - z_n) \\ & + q_z^{m,n} \pi (R_{m+1}^2 - R_m^2) - q_z^{m,n+1} \pi (R_{m+1}^2 - R_m^2) \end{aligned}$$

where:

$$q_{\rho}^{m,n} = \frac{T_{m-1,n} - T_{m,n}}{\frac{R_m - R_{m-1}}{2\lambda_{m-1,n}} + \frac{R_{m+1} - R_m}{2\lambda_{m,n}}}$$

and

$$q_z^{m,n} = \frac{T_{m,n-1} - T_{m,n}}{\frac{z_n - z_{n-1}}{2\lambda_{m,n-1}} + \frac{z_{n+1} - z_n}{2\lambda_{m,n}}}$$

(27)

The parameter λ may include dispersion effects, as described in Section III.2.1. The time step Δt is chosen so as to ensure numerical stability of the solution.

During the storage and rest period no translation of the temperature field occurs and heat transfer is purely by conduction. During the production period, the convection is treated as during the injection period. The length of the production period, t_p , is given as input. For every timestep, t_p/M , the temperature distribution is shifted one element toward the well, and the temperatures from all the elements directly adjacent to the well are weighted according to their heat capacity and averaged to give the production temperature. If t_p is different from t_i , the fluid flow rate will be adjusted so that the volumes of water injected and produced will remain fixed, i.e., $Q_i t_i = Q_p t_p$.

Figure 2 shows the temperature distributions at various times during the first cycle as generated by the SFM with and without conduction to illustrate the superposition of conduction and convection. A typical mesh consists of about 1000 elements. Nearly 300 different cases have been simulated, with M ranging from 10 to 40. The computer time required for a typical annual cycle is about 15 seconds on a CDC 7600.

III. Results

The results of the large number of different ATEs systems that have been simulated using the steady flow model are presented in graphical form. Section III.1 shows the dependence of the thermal behavior on the dimensionless groups derived in section II.3, as well as the dependence on some of the individual parameters that make up the dimensionless groups. Section III.2 discusses the effect of a velocity-dependent dispersion, unequal length periods, finite cap-rock, long term behavior, and multilayer flow.

III.1. Dependence on Parameters of the Dimensionless Formulation

In Section II.3 it was shown that the recovery factor is a function of five dimensionless parameters. One of these is the number of cycles. The recovery factor increases as the number of cycles increases, with the increment decreasing for later cycles. The results given in the following sections (III.1.1 and III.1.2) are for the first and fifth cycles. Long term effects are discussed in Section III.2.3.

Another parameter, the ratio between heat capacity in the aquifer and heat capacity in the confining layers, C_a/C_c , varies within a small range and is mainly determined by the water content (or porosity) of the two layers. The correspondingly small variation of the recovery factor with respect to the capacity ratio, which is shown in Figure 3, is largest when Λ and λ_a/λ_c are small. The results which follow are given for C_a/C_c equal to 1.25, i.e., when the aquifer has a higher water content (porosity) than the confining layers.

III.1.1 Results in Terms of Dimensionless Groups

Of the five dimensionless parameters introduced in Section II.3, the effects of three of them, Pe , Λ , and λ_a/λ_c , are more critical and remain to be examined. The range of Pe and Λ is chosen with respect to conditions met in seasonal or daily storage. The ratio between thermal conductivity in the aquifer and the confining layers, λ_a/λ_c , depends largely on the magnitude of dispersive effects caused by the flow in the aquifer. Dispersion is discussed in Section III.2.2.

III.1.1.1 Recovery Factor

Figures 4 - 9 show the energy recovery factor as a function of Pe and Λ for the first and fifth cycles. Three different values of the thermal con-

ductivity ratio, λ_a/λ_c , have been used. The sensitivity of the recovery factor to λ_a/λ_c is most pronounced for small values of the Pe and Λ numbers. Additionally, for a given λ_a/λ_c the large initial increase in recovery factor with increases of Pe and Λ is followed by a more gradual increase. Hence, the recovery factor is most sensitive to a change in the parameters λ_a/λ_c , Pe and Λ at small values of Pe and Λ .

III.1.1.2 Production Temperatures

The temperature of the water extracted during the production period of the first and fifth cycles is shown in Figures 10 - 12 for different combinations of Pe, Λ , and λ_a/λ_c . For values of Pe larger than 200, production temperature shows little dependence on Pe.

To demonstrate the effect of a cut-off temperature, consider the case with $\lambda_a/\lambda_c = 1$, Pe = 20, $\Lambda = 50$. From figure 4, the first cycle recovery factor is 0.59. From figure 10, the final dimensionless production temperature for the first cycle is about 0.3. For an application that can only use energy above $T'_{ref} = 0.25$, equation 6 gives $\varepsilon_{ref} = 0.45$. If T'_{ref} were greater than 0.3 equation 6 would underestimate ε_{ref} .

III.1.2 Results in Terms of Individual Parameters

In order to show the explicit dependence on certain physical parameters a number of cases have been studied in more detail.

III.1.2.1 Reference Case

The following parameters are used in the reference case: aquifer thickness -- 50m, injection volume -- 60,000 m³, an annual cycle, no dispersion, and an infinitely thick caprock.

These parameters are summarized in Table 1, which also shows the values of the dimensionless groups formed from these parameters -- $Pe = 39.6$, $\Lambda = 396.4$, $\lambda_a/\lambda_c = 1$, $C_a/C_c = 1.25$.

The thermal volume is $V = 98,000 \text{ m}^3$. Unless otherwise noted, reference case parameters are always used.

The recovery factors for the first five cycles are:

year	1	2	3	4	5
ϵ	0.77	0.81	0.83	0.84	0.85

Figure 13 shows the temperature of extracted water during the production period.

As an illustration of the size of the reference case, a average single family house in the U.S.A. requires about 15,000 kWh of energy for heating during one year. Let us assume that the storage system operates with a temperature difference of 25°C . If the recovery factor is about 0.8, and if half of the total energy requirement is met with stored energy, the reference aquifer should suffice for 180 houses.

III.1.2.2 Volume

The size of the heated region in the aquifer is a fundamental parameter of the storage system. Figure 14 gives the recovery factor as a function of cycle number for several thermal volumes with the shape of the thermal volume kept the same in all cases, a cylinder with an aspect ratio, H/R , of 1. The amount of stored heat is proportional to the thermal volume; the heat losses to surrounding material take place through the surface of this volume. Therefore the relative heat loss is roughly proportional to the surface to volume

ratio, which is $2/R + 2/H$. This ratio decreases and thus becomes more favorable as the thermal volume increases.

The temperature of the extracted water during the first production period is shown in Figure 14. In the case where $V = 3,100,000 \text{ m}^3$ the initial slope of the curve reflects the vertical heat loss to the confining layers. The faster decrease in the temperature curve after 60 days is due to the radial heat loss in the aquifer. When the volume becomes much smaller, the radial heat loss affects the temperature of the extracted water during the whole production period.

III.1.2.3 Shape

Although the recovery factor increases with the thermal volume, there is one optimal aspect ratio, or shape, for which the recovery factor attains a maximal value for each volume. Figure 15 shows recovery factor as a function of aspect ratio for the first five cycles. The curves have a rather flat maximum at an aspect ratio of 1.5. The first cycle production temperature as a function of time for different values of the aspect ratio are given in Figure 16. If the thermal conductivity of the confining layers is decreased, the maximal recovery factor is obtained for a somewhat smaller aspect ratio. This is shown in Figure 17. The difference between the recovery factors in these cases is, of course, most pronounced for small aspect ratios, when the area facing the confining layers is relatively large.

Some insight into the variation of the optimal aspect ratio may be gained by considering the following expression, which gives a rough approximation for the first cycle recovery factor. The heat loss per unit area across the plane interface between two semi-infinite media originally at different tem-

peratures in a time τ (Carslaw and Jaeger, 1959) is multiplied by the surface area of a cylinder of thickness H and radius R . This yields:

$$\epsilon = 1 - \frac{2}{C_a} \sqrt{\frac{\tau}{\pi}} \left(\frac{\sqrt{\lambda_a C_a}}{R} + \frac{\sqrt{(\lambda C)_f}}{H} \right)$$

where

$$(\lambda C)_f = \left(\frac{2}{1/\sqrt{\lambda_a C_a} + 1/\sqrt{\lambda_c C_c}} \right)^2 \quad \text{and } \tau = (t_i + t_p)/2 + t_s \quad (28)$$

The significance of τ is discussed in Section III.2.2. The factor $\sqrt{(\lambda C)_f}$ is the harmonic mean of the aquifer and confining layer $\sqrt{\lambda C}$ values. The first term of equation 28 in parentheses is proportional to horizontal heat loss, the second to vertical heat loss. This approximation always underpredicts recovery factor and is worse for small recovery factors. For the reference case, it is .03 less than the numerically simulated value of .77. For a recovery factor of .48, it is .34. The method of Lagrange multipliers is used to find the aspect ratio which maximizes ϵ for a given volume. This optimal aspect ratio is:

$$\frac{H}{R} = 2 \sqrt{\frac{(\lambda C)_f}{\lambda_a C_a}} \quad (29)$$

Thus, the variation of the optimal aspect ratio with thermal properties is slow.

In practice, the choice of aquifer may be limited, thus fixing the aquifer thickness and the thermal properties of the system. Also, seasonal energy supply and demand may determine the length of cycle time periods. In this case, the volume of injected water is the only parameter with which to optimize the recovery factor. As the thermal volume becomes larger, the

recovery factor initially increases rapidly, then levels off. The initial rapid increase occurs before the thermal radius attains the value which yields the optimal aspect ratio for that aquifer thickness.

When the volume of the injected water is limited and small compared to the thickness of the aquifer, it may be advantageous to use a well that penetrates only a part of the aquifer, in order to get a more compact shape of the heated region. However, the use of partial penetration may lead to increased mixing of hot and cold water in the aquifer, which will lower the recovery factor.

If the quantity of energy to inject is fixed, one possibility is to inject a larger volume of water at a lower temperature. This will increase the recovery factor provided that the energy content is calculated using the original ambient temperature as a reference. It may reduce problems related to thermal stratification and water chemistry. However, a decrease in energy quality (temperature) is unacceptable in many applications.

III.1.2.4 Aquifer Thermal Conductivity

Heat loss in the aquifer is due to the mixing of cold and warm water (dispersion, discussed in Section III.2.1), and heat conduction. The recovery factor for the first five cycles is given for a number of different thermal conductivity values in Figure 18. Figure 18 also shows the corresponding temperature of the extracted water during the first cycle production period. Figure 19 gives the recovery factor as a function of the thermal conductivity.

The range of thermal conductivity shown in these plots, up to $\lambda_a = 20 \text{ J/msK}$ is larger than would be likely to be measured on a laboratory sample of aquifer material. However, as will be discussed in the next section, dispersion may contribute to a large effective thermal conductivity in the aquifer.

Figures 18 and 19 show dependence on aquifer thermal conductivity for cases with aspect ratio, H/R , near the optimal value. For a system with $H/R \ll 1$, vertical heat losses will dominate and recovery factor will be nearly independent of aquifer thermal conductivity.

III.2 Dependence on Factors Not Accounted for in the Dimensionless Formulation

This section deals with several factors which influence the behavior of an ATEs system, which are not included in equations 7 and 8.

III.2.1 Velocity-Dependent Dispersion

During periods when the water flows through the aquifer there is, in addition to ordinary heat conduction, a dispersion of heat due to the velocity distribution across each flow channel, the irregularity of the pore system, and large scale aquifer heterogeneities. According to the theory for dispersion of a non-adsorbent tracer in uniform porous media (Scheidegger, 1960), the dispersion is proportional to $|\underline{v}_p|^m$, where \underline{v}_p is the pore velocity. The value of m ranges from 1 to 2. When m is 1 the molecular transverse diffusion between adjacent streamlines can be neglected, and when m is 2 the transverse diffusion is important. The transverse diffusion becomes more important as pore velocity decreases. The thermal conductivity of the stagnant liquid-solid mixture and the heat dispersion are combined to form an effective thermal conductivity.

Generally, the effective thermal conductivity is a tensor. However, we will assume that for our mesh design, the off-diagonal elements are zero and the effective thermal conductivity has different values parallel to and perpendicular to the direction of fluid flow. The effective thermal conductivity is written in terms of the Darcy velocity, which is the product of the pore velocity and the aquifer porosity. When $m = 1$ we have:

$$\tilde{\lambda}_{a_{\parallel}} = \lambda_a + d_{\parallel} \cdot |v| \cdot C_w \quad (30)$$

$$\tilde{\lambda}_{a_{\perp}} = \lambda_a + d_{\perp} \cdot |v| \cdot C_w$$

and when $m = 2$:

$$\tilde{\lambda}_{a_{\parallel}} = \lambda_a + d_{\parallel}^* \cdot |v|^2 \cdot C_w \quad (31)$$

$$\tilde{\lambda}_{a_{\perp}} = \lambda_a + d_{\perp}^* \cdot |v|^2 \cdot C_w$$

The parameters d_{\parallel} , d_{\perp} , d_{\parallel}^* , d_{\perp}^* are properties of the aquifer; d_{\parallel} and d_{\perp} are often referred to as dispersion lengths. Laboratory experiments have shown that d_{\perp} is an order of magnitude smaller than d_{\parallel} for most field samples. We have found that the recovery factor and production temperature exhibit only a weak dependence on the value of d_{\perp} and d_{\perp}^* . This weak dependence is supported by equation 28, the analytical approximation for recovery factor, in which the vertical heat loss is proportional to $\sqrt{(\lambda C)_f}$ (now more properly defined as $\sqrt{(\lambda C)_f} \cong 2/[1/\sqrt{\tilde{\lambda}_{a_{\perp}} C} + 1/\sqrt{\lambda C}]$). Even if d_{\perp} or d_{\perp}^* were to increase $\tilde{\lambda}_{a_{\perp}}$ significantly, the change in $\sqrt{(\lambda C)_f}$ would be relatively small.

First we consider the case where $\tilde{\lambda}_a$ is linearly dependent on v (equation 30). Figures 20 and 21 show recovery factor and production temperature as d_{\parallel}

is varied. The dependence of the recovery factor on d_{\parallel} appears to be very similar to that for λ_a (Figures 17 and 19). The thermal conductivity used to obtain Figures 18 and 19 can be considered to be a scalar effective conductivity of the form:

$$\tilde{\lambda}_a = \lambda_a + \lambda_d$$

where λ_d is a constant addition to the thermal conductivity to account for dispersion. To further examine the effect of the velocity dependence in $\tilde{\lambda}_a$, Figure 22 shows the first cycle production temperature for three cases which all have a recovery factor of 0.60, but which use three different formulas to describe the dispersion (equations 30, 31, and 32). Clearly the production temperature curves are very similar. For later cycles the recovery factors and production temperature curves begin to diverge slightly.

The magnitude of the tracer dispersion lengths vary within a wide range, but may be determined by a tracer injection experiment in the field. Experimental data show that tracer and heat dispersion lengths (d_{\parallel} , d_{\perp}) are practically identical for flow in a uniform material (Bear, 1972). For the parameter ranges considered in this study, we obtained the empirical relation:

$$\tilde{\lambda}_a = \lambda_a + 0.3 \frac{d_{\parallel} RC_a}{t_i} \quad (33)$$

between the scalar effective thermal conductivity, which is used for the whole ATES cycle, and the dispersion length d_{\parallel} .

Equation 33 was generated by running the SFM for a range of the parameters R , H , t_i , λ_a , C_a , using equations 30 and 32 to describe dispersion effects, and correlating cases with equal recovery factors. The ratio $d_{\parallel}/d_{\perp} = 10$ was used. Different values of d_{\perp} do not change equation 33 appreciably.

Figures 21 and 22 have shown that the recovery factor and production temperature are strongly dependent on dispersion. However, the dimensionless groups used to predict thermal behavior came from equations that do not include dispersion. As we have shown in this section, dispersion acts to create a large effective aquifer thermal conductivity. Hence, $\tilde{\lambda}_a$ may be used instead of λ_a in Pe and λ_a/λ_c to account for dispersion.

The effect of the addition of dispersion to the thermal conductivity may be observed by comparing Figures 4 and 6, and Figures 10 and 12. For example, consider a case with $Pe = 50$, $\Lambda = 50$, and $\lambda_a/\lambda_c = 1$; an increase of effective thermal conductivity by a factor 10 to include dispersion changes the value of the parameters to $Pe = 50$, and $\tilde{\lambda}_a/\lambda_c = 10$. This reduces the first cycle recovery factor from 0.67 to 0.40. The decrease in production temperatures is also substantial.

III.2.2 Unequal Length Periods

The recovery factor depends on the length of the cycle, t_c , and the intracycle scheduling—the relative duration of injection, storage, production, and rest periods. Figure 23 shows the first cycle recovery factor as a function of t_c for different schedules for three thermal volumes. In case A the fluid is injected during the first half of the cycle and produced during the second half. There is no storage or rest period. Case B refers to a cycle which is subdivided into equal injection, storage, production, and rest periods. Case C consists of a hypothetical cycle with instantaneous injection and production. Here, the durations of the injection and production periods are zero, while the storage and rest periods are each a half cycle. For a given t_c , the recovery factor is higher for a shorter storage period, t_s .

The results of Section III.1 were calculated for a cycle with equal lengths, t_i , of the individual periods. In order to use the Section III.1 figures for cases where the different periods have unequal durations, a time measure more suitable than t_i is required. An adequate measure is the time an injected water particle resides in the aquifer, averaged over all particles in the injection volume. This time, called τ , is given by:

$$\tau = \frac{1}{2}(t_i + t_p) + t_s \quad (34)$$

provided that the flow is constant during the injection and production periods. To allow for any scheduling, the time t_i , is replaced by $\tau/2$ in the formulas for Pe , Λ , $\tilde{\lambda}_a$, and the finite thickness caprock effect (equations 21, 33, 36, and 37). The error made by using the recovery factor curves of section III.1 with $\tau/2$ is small. According to Figure 23, the largest departure from Case B causes a change in recovery factor of less than 5%. Variation in scheduling affects the production temperature more strongly. When there is no storage period, the production temperature begins at T_1 ; with a storage period, the production temperature begins below T_1 , but decreases more slowly.

When the aquifer and confining layer thermal properties are the same, the first cycle recovery factor for Case C can be determined analytically. The recovery factor is given by the formula for the mean temperature decline in a cylinder, which is shown in Appendix B.

III.2.3. Finite Thickness Caprock

The vertical heat loss from a shallow aquifer system may be substantially enhanced due to the influence of the ground surface, acting as a constant temperature boundary. A caprock with thickness D can be accounted for in the

dimensionless formulation discussed in Section II.3, by forming another dimensionless parameter:

$$\left(\frac{D}{L}\right)^2 = \frac{D^2}{\frac{\lambda_a}{\lambda_c} \frac{\lambda_c t_i}{c_c}} \quad (35)$$

Because of the small interdependence of radial and vertical losses, $D = \infty$ is used for the plots in Section III.1.1, and the effect of a finite caprock thickness is discussed here separately.

The key parameter in the formula describing the finite caprock effect is $d = D/H$. Figures 24 - 26 show the recovery factor for an aquifer with a finite caprock relative to that with an infinite caprock, $\epsilon(d)/\epsilon(\infty)$, as a function of $1/\Lambda$. The figures display results for various values of d , for the first and fifth cycles, and for $\lambda_a/\lambda_c = 1, 2, \text{ and } 10$. Hence the recovery factor for the finite caprock cases can be calculated by using the appropriate figure which gives the recovery factor for the infinite caprock (Figures 4 - 9), and then multiplying the result by the number obtained from Figures 24, 25 or 26.

Several observations may be made about Figures 24-26. For a relatively thick caprock ($d > .5$), vertical heat loss is primarily determined by the aquitard thermal properties, but there is a marked increase in the effect of λ_a as d decreases. The thickness of the aquifer, H , appears both in d and in $1/\Lambda$. The parameter d decreases as $1/H$, and $1/\Lambda$ decreases as $1/H^2$; an increase in H yields an increase in $\epsilon(d)/\epsilon(\infty)$. On the other hand, $\epsilon(d)/\epsilon(\infty)$ initially decreases as the number of cycles increases, then reaches steady state. The number of cycles required for $\epsilon(d)$ to reach steady state is proportional to D , and decreases as λ_a/λ_c increases.

We have found that if either of the following conditions holds, then the finite caprock effect will be small (less than a 5% reduction of the fifth cycle recovery factor):

$$(1) \quad \left(\frac{D}{L}\right)^2 > 10, \quad \Lambda > 2 \quad (36)$$

$$(2) \quad \Lambda > 300, \quad \text{any } D \quad (37)$$

When the first condition holds, the thickness of the caprock is so large that the effect of the surface is not appreciably felt by the aquifer. When the second condition holds, the aquifer is thick enough that the heat loss to the ground surface results in only a minor change in the aquifer heat content. When the aquifer and confining layer thermal properties are the same, the mean temperature decline formula for a cylinder with a finite caprock can be used to obtain an analytical solution for the finite thickness caprock effect on recovery factor for the first cycle. This is shown in Appendix C.

III.2.4 Long-term Effects

The transient energy loss for each cycle decreases as the number of cycles increases, so that the recovery factor improves. Figure 27 shows the recovery factors for 33 annual cycles for an aquifer with an infinitely thick caprock and with a relatively thin caprock ($D/H=0.1$). The increase in recovery factor is quite rapid during the first few cycles for both cases, but the thin caprock case approaches steady state faster.

During each cycle, energy is lost from the injected water to the surroundings. If the aquifer may be used for purposes other than heat storage, the thermal pollution caused by the residual heat may be a problem. The radial distance from the well to a certain isotherm at the

end of each storage cycle is given in Figure 28 for the infinite and finite caprock cases. The isotherms give a rough outline of the radial distribution of the residual heat just before the injection period of the next cycle starts. As expected, in the thin caprock case, with heat lost to the surface, the radial extent of the residual heat is lessened, and can be seen approaching a constant value.

The radial distance at which the temperature increase equals 10% of the temperature difference between injected and ambient water has not reached farther than 47 meters after 33 cycles for the infinite caprock case. At this time the rate at which this distance increases is only 0.4 meters per year. The residual heat is spreading out in the aquifer at a slow rate. In this example the thermal conductivity in the aquifer is only 2.5 J/msK, which is a rather low value. Of course in these calculations we have not considered the possible presence of faults or other heterogeneity factors that may serve as special channels for fluid flow.

The effect of regional flow has not been considered in this study. However, since the rate at which residual heat spreads is very low in the case of no regional flow, one may assume that the magnitude of the regional flow is very important when estimating thermal pollution.

III.2.5 Multiple Layers with Different Flowrates

Buoyancy flow induced by the density difference between hot and cold water is discussed briefly in Appendix A. While the steady flow model does not solve the coupled heat and mass transfer equations, the final effect of buoyancy flow is a tilted thermal front. When $H/R < 4$, the surface area of the hot region is increased when the thermal front is tilted. If the tilting

is extreme, during production unheated native water in the lower part of the aquifer will be recovered along with heated water. Both these effects lower the recovery factor, so it is desirable to examine them. A tilted front can be generated roughly by multiple layers with different specified horizontal flowrates within the SFM.

As an example of this technique, we consider a three-layered case, where the flowrate during injection is enhanced in the upper layer and reduced in the lower layer. The flowrate during production is the same in all layers. Figure 29 shows the production temperature for three cases with different combinations of flowrates in the layers, as indicated by the accompanying figures. The aquifer has a thickness of 20 meters. The total flow is the same in all cases. Curve A represents the case when the flow rate is the same in the three layers. The recovery factor is 0.65. In case C, where the tilting angle after the injection period is close to 45 degrees, the recovery factor is reduced to 0.58. Figure 30 shows a similar example with four cases in a 50 meter thick aquifer. The recovery factor decreases from 0.77, when the flow is the same in all layers (case A), to 0.63 in case D, where the tilting angle is close to 45 degrees.

The permeability of the aquifer must be quite low in order that the tilting angle does not exceed 45° during the storage cycle (Hellström et al., 1979).

IV. Comparisons with Field Experiments

The use of the results presented in Section III is illustrated by comparing these results with the recovery factors and production temperatures for two recent ATEs field experiments.

IV.1 Auburn

The Water Research Institute at Auburn University, Auburn, Alabama has performed a two cycle ATES field experiment using a 21 m thick aquifer with an ambient temperature of 20°C (Molz et al., 1981). Although the top of the storage aquifer lies 40 m below the ground surface, it is overlain by a 9 m thick clay layer, above which is a shallow aquifer, whose temperature remained constant throughout the experiment. The injection/production well penetrated the middle 9 m of the aquifer.

During each six month cycle, 55,000 m³ of water was injected at 55°C, stored, and recovered. The recovery factors for the two cycles were 66 and 76 percent.

Independent modeling work (Tsang, Buscheck and Doughty, 1980; Buscheck, Doughty and Tsang, 1981), using a coupled heat and mass transfer numerical model, has matched the simulated and observed aquifer temperature fields at the end of the first injection period. It indicates that an effective conductivity $\tilde{\lambda}_a = 2\lambda_a$ is appropriate for this experiment. A summary of the parameters needed is shown in Table 1. Also shown are the dimensionless groups used to predict recovery factor: $Pe = 78.4$, $\Lambda = 80.3$, $\tilde{\lambda}_a/\lambda_c = 2$, and $d = 0.4$.

The first cycle finite caprock effect, shown in Figure 25, is negligible. Hence, the first cycle recovery factor is estimated from Figure 6 to be 0.71. One of the effects of the partially penetrating injection/production well may be shown the following way. From temperature observations made in the aquifer, the thermal radius reached 43 m, which implies the effective thickness of the aquifer was 16 m. Using $R = 43$ and $H = 16$ gives $Pe = 101.9$, $\Lambda = 46.6$, $d = 0.5$. Using these values in Figures 25 and 6 yields $\epsilon = 0.68$. The decrease from 0.71 to 0.68 is due to the worsening of the aspect ratio. Experimental observations

also indicated some thermal front tilting. According to equation A1, the characteristic tilting time, t_0 , is 28 days, to be compared with a τ of 110 days. Hence, the observed first cycle recovery factor, 0.66, may be lower than that predicted due to buoyancy flow.

IV.2 Bonnaud

The Bureau de Recherches Geologiques et Minieres, Orleans, France has conducted a four cycle experiment on a 2.5 m thick aquifer with ambient temperature 12.5°C at Bonnaud, France (Menjoz and Sauty, 1980). During each 12 day cycle, 490 m³ of water was injected at 35°C and recovered. The fourth cycle recovery factor was 67.7%. A summary of needed parameters is shown in Table 1. Also shown are the dimensionless groups used to predict recovery factor: $Pe = 15.4$, $\Lambda = 25.2$, $\tilde{\lambda}_a/\lambda_c = 13$, and $d = 1.6$. The curves for $\tilde{\lambda}_a/\lambda_c = 10$ are used to predict the recovery factor. The fifth cycle caprock effect, shown in Figure 26, is about 0.99. From Figure 9, the fifth cycle infinite caprock recovery factor is 0.65. Combining these two yields $\epsilon = 0.64$. The fourth cycle recovery factor would be slightly smaller. This underpredicts the observed fourth cycle recovery factor of 0.677. The difference is due, at least in part, to the scheduling, as discussed in Section III.2.2.

V. Summary

The thermal behavior of an aquifer thermal energy storage system which consists of a single well in an infinite horizontal aquifer has been studied. The heat transfer equations are presented in dimensionless form in order to identify the set of parameters which define the system's thermal behavior. A numerical model in which a steady fluid flow is prescribed in the radial direction is used to run numerical simulations of ATEs cycles. The net thermal

behavior of the storage system is given by the recovery factor and the time-dependent temperature of the recovered water. The recovery factor is defined as the quotient between recovered and injected energy; the energy is calculated using the initial groundwater temperature as a reference. The effects of buoyancy flow are neglected in this study, thus the results should be applicable to a system with either low-permeability, small temperature difference, short cycle lengths or small aquifer thickness. A number of parameters have been varied in order to estimate their effect on the thermal behavior.

VI. Conclusions

The main conclusions are summarized below:

- o The storage volume is a fundamental parameter of the system. The relative heat loss is roughly proportional to the surface to volume ratio. Even for an optimal aspect ratio for our reference case, a minimal injection volume of about 50,000 m³ is required in order to obtain a good recovery factor (0.7) during the first annual cycle. For other cases, similar minimal volumes can be estimated using the figures in Section III. The aquifer storage concept for a seasonal cycle must be applied on a large scale in order to ensure a high recovery.
- o The thermal behavior of the storage system is very sensitive to the value of the effective thermal conductivity in the aquifer. The effective thermal conductivity is defined to include a contribution from dispersion which may be quite large.
- o After an initial transient period, the heat loss through the upper surface of the aquifer is determined by the thickness of the caprock. The transient period may be quite long. The effect of a finite caprock on the fifth cycle recovery factor is less than 5% if $(D/L)^2 > 10$ and $\Lambda > 2$.

Further, the influence of the finite caprock loss decreases as the thickness of the aquifer increases.

o The cycle is divided into periods of injection, storage, production, and rest in accordance with the supply and demand of heat. The relative duration of these periods appears to have a fairly small influence on the recovery factor, when the length of the cycle is constant. A parameter $\tau = (t_i + t_p)/2 + t_s$ is defined as the average length of time an injected fluid particle spends in the aquifer. For cases with periods of unequal length, $\tau/2$ may be used in place of t_i in the formulas for Pe , Λ , $\tilde{\lambda}_a$, and D/L .

o The recovery factor increases with the number of storage cycles. During each cycle heat is lost to the cold surroundings. The increasing amount of residual heat improves the performance of the storage systems during the next cycle. However, the residual heat may be in conflict with other uses of the aquifer. The thermal pollution appears to spread out at a rather slow rate, when there is no regional flow in the aquifer.

o The shape of the heated volume should be as compact as possible in order to minimize the heat loss. The recovery factor has a rather flat maximum when the radius of the heated volume is about 2/3 of the aquifer thickness.

Acknowledgement

This work was supported by the Assistant Secretary of Conservation and Solar Energy, Office of Advanced Conservation Technology, Division of Thermal and Mechanical Storage Systems of the U. S. Department of Energy under contract W-7405-ENG-48. This report represents work performed within the Seasonal Thermal Energy Storage program managed by Pacific Northwest Laboratory. On the Swedish side, the work has been supported by the National Swedish Board for Energy Source Development (NE).

NOMENCLATURE

A surface area of the (m,n)th mesh element (m^2)

C volumetric heat capacity ($\frac{J}{m^3 K}$)

$C_a = \phi_a C_w + (1-\phi_a)C_r$ aquifer volumetric heat capacity ($\frac{J}{m^3 K}$)

$d = \frac{D}{H}$ ratio of caprock thickness to aquifer thickness

d_{\parallel}, d_{\perp} first order dispersion constants, dispersion lengths, (m)

$d_{\parallel}^*, d_{\perp}^*$ second order dispersion constants (s)

D caprock thickness (m)

H aquifer thickness (m)

k, k' horizontal and vertical aquifer permeabilities ($\frac{m^2}{s}$)

$L = \sqrt{\frac{\lambda_a \lambda_c t_i}{\lambda_c C_c}}$ characteristic length (m)

M number of mesh elements in each row between $\rho = 0$ and R

$Pe = \frac{C_a R^2}{2\lambda_a t_i}$ Peclet number

q heat flowrate per unit area ($\frac{J}{m^2 s}$)

Q volumetric fluid flowrate ($\frac{\text{m}^3}{\text{s}}$)

R thermal radius (m)

$R_m = \sqrt{\frac{m-1}{M}} R$ distance to the inner edge of the m th column of mesh elements (m)

t time (s)

$t' = \frac{t}{t_i}$ dimensionless time

$t_c = t_i + t_s + t_p + t_r$ length of one cycle (s)

t_0 characteristic tilting time (s)

Δt timestep for conduction (s)

T temperature (K)

T_0 original ambient temperature (K)

T_1 injection temperature (K)

$T' = \frac{T - T_0}{T_1 - T_0}$ dimensionless temperature

T_p production temperature (K)

\bar{T}_p production temperature averaged over production period (K)

$\bar{T}'_p = \epsilon$ dimensionless average production temperature

T_m mean temperature in a cylinder (K)

T_{ref} reference (cutoff) temperature (K)

v_p pore velocity ($\frac{m}{s}$)

$v = \frac{Q}{2\pi H\rho}$ steady radial darcy velocity ($\frac{m}{s}$)

$V = \pi R^2 H$ thermal volume (m^3)

$V_{m,n}$ volume of the (m,n)th mesh element (m^3)

$V_w = Q_i t_i = Q_p t_p = (C_a/C_w)V$ volume of water injected and produced (m^3)

z vertical coordinate (m)

$z' = z/L$ dimensionless z

z_n vertical distance from the top of the caprock to the top of the nth row of mesh elements (m)

ϵ recovery factor, ratio of produced to injected energy, with energies measured relative to T_0

ϵ_{ref} recovery factor with energies measured relative to T_{ref}

$\kappa = \frac{\lambda}{C}$ thermal diffusivity ($\frac{m^2}{s}$)

λ thermal conductivity ($\frac{J}{msK}$)

$\tilde{\lambda}_{a_{\parallel}}, \tilde{\lambda}_{a_{\perp}}$ effective aquifer thermal conductivity, of the form $\tilde{\lambda}_a = \lambda_a + \text{dispersion term } (\frac{J}{msK})$, where the dispersion term may be:

λ_d constant, in which case $\tilde{\lambda}_{a_{\parallel}} = \tilde{\lambda}_{a_{\perp}} \equiv \tilde{\lambda}_a$

$d_{\parallel} | v | C_w, d_{\perp} | v | C_w$ first order velocity dependent

$d_{\parallel}^* | v |^2 C_w, d_{\perp}^* | v |^2 C_w$ second order velocity dependent

$$\sqrt{(\lambda C)_f} = \frac{2}{\frac{1}{\sqrt{\lambda_c c_a}} + \frac{1}{\sqrt{\lambda_c c_c}}}$$

effective $\sqrt{\lambda C}$, harmonic mean of aquifer and confining layer values $\left(\frac{J}{m^2 s^{1/2} K}\right)$

$$\Lambda = \frac{c_a^{2H^2}}{\lambda_c c_c t_i} \quad \text{Lambda number}$$

μ_0, μ_1 viscosity of ambient and injected water $\left(\frac{kg}{ms}\right)$

ρ radial coordinate (m)

$\rho' = \frac{\rho}{L}$ dimensionless ρ

ρ_0, ρ_1 density of ambient and injected water $\left(\frac{kg}{m^3}\right)$

ϕ porosity

$\tau = (t_i + t_p)/2 + t_s$ effective time a fluid particle spends in the aquifer(s)

Subscripts

a	aquifer
c	confining layer
r	rock
w	water
ρ	radial
z	vertical
m	label for mth column of elements in mesh
n	label for nth row of elements in mesh
m,n	label for the (m,n)th element in mesh (also used as a superscript)
i	injection
s	storage
p	production
r	rest
c	cycle

Appendix A - Buoyancy Tilting

The density difference between hot and cold water induces a buoyancy flow of the hot water towards the upper part of the aquifer. An order of magnitude estimate of the tilting rate of a more or less vertical front may be deduced from the following idealized case (Hellström et al., 1979). Consider a sharp, vertical thermal front in a confined aquifer (Figure A1). The aquifer layer has an infinite horizontal extension. The vertical permeability, k' , may differ from the horizontal permeability, k . The tilting rate is given by a characteristic tilting time, t_0 , which is:

$$t_0 = 0.034 \cdot \frac{H}{\sqrt{kk'}} \cdot \frac{C_a}{C_w} \cdot \frac{(\mu_0 + \mu_1)}{(\rho_0 - \rho_1)} \quad (A1)$$

The buoyancy tilting of an initially vertical front during a time t_0 is about 60° . The most important factors are the temperature levels, which determine μ and ρ , and the permeability. If the time of the cycle is smaller than t_0 , then the tilting is expected to be moderate.

The time constant, t_0 , was derived for the plane case, but the magnitude does not change appreciably for the radial case. If the thermal front is diffuse, rather than sharp, the tilting rate is slightly lowered. Furthermore, as the thermal front tilts, the flow resistance in the hot part of the aquifer is reduced because of the lower viscosity of hot water. Forced convection, then, gives an increase of the tilting rate during injection periods, and a decrease during production periods for hot water storage. For chilled water storage, forced convection decreases the tilting rate during injection and increases it during production.

Appendix B. Mean Temperature Decline in a Cylinder

Let us assume that the storage volume has the shape of a cylinder with radius, R , and height, H . Initially, the temperature is T_1 throughout this volume and T_0 in the surrounding, infinite medium. The whole system is assumed to have homogeneous thermal properties, with thermal conductivity λ , heat capacity per unit volume C , and thermal diffusivity $\kappa = \lambda/C$. The temperature field is governed by the ordinary heat equation.

The mean temperature in the storage volume, T_m , at a time t is given by a product solution (Claesson, Efring and Hellström, 1980) namely:

$$T_m(t) = T_0 + (T_1 - T_0) \cdot g_m\left(\frac{\kappa t}{R^2}\right) \cdot f_m\left(\frac{4\kappa t}{H^2}\right) \quad (\text{B1})$$

where the radial factor is:

$$g_m(x) = 1 - e^{-\frac{1}{2x}} \left[I_0\left(\frac{1}{2x}\right) + I_1\left(\frac{1}{2x}\right) \right] \quad (\text{B2})$$

and the vertical factor is:

$$f_m(y) = \text{erf}\left(\frac{1}{\sqrt{y}}\right) - \sqrt{\frac{y}{\pi}} \cdot \left(1 - e^{-\frac{1}{y}}\right) \quad (\text{B3})$$

Here I_0 and I_1 are modified Bessel functions and erf is the error function.

The following approximations may be used:

$$g_m(x) \approx 1 - 2\sqrt{\frac{x}{\pi}} \quad x \ll 1 \quad (\text{B4})$$

$$g_m(x) \approx \frac{1}{4x} \left(1 - \frac{1}{4x}\right) \quad x \gg 1 \quad (\text{B5})$$

$$f_m(y) \approx 1 - \sqrt{\frac{y}{\pi}} \quad y \ll 1 \quad (\text{B6})$$

$$f_m(y) \approx \frac{1}{\sqrt{\pi y}} \left(1 - \frac{1}{6y}\right) \quad y \gg 1 \quad (\text{B7})$$

The recovery factor for the first cycle can be estimated by substituting τ for t in equation B1, where the time constant τ is:

$$\tau = (t_i + t_p)/2 + t_s \quad (\text{B8})$$

The recovery factor becomes:

$$\epsilon = g_m \left(\frac{kT}{R^2} \right) \cdot f_m \left(\frac{4kT}{H^2} \right) \quad (\text{B9})$$

Figure B1 shows the recovery factor as a function of the parameters

$$\frac{R}{\sqrt{kT}} = \sqrt{Pe} \quad \text{and} \quad \frac{H}{\sqrt{kT/2}} = \sqrt{\Lambda} \quad .$$

Appendix C. Influence of a Finite Caprock on the Mean Temperature Decline

The effect of a finite caprock of thickness D can be analyzed using the method described in Appendix B and the superposition principle (Claesson, et al., 1980). The function f'_m , which gives the vertical effects, includes the dependence on the finite thickness of the caprock, that is:

$$f'_m(d, y) = f_m(y) + \sqrt{y} \cdot \text{ierfc} \left(\frac{2d + 1}{\sqrt{y}} \right) - \frac{\sqrt{y}}{2} \left[\text{ierfc} \left(\frac{2d + 2}{\sqrt{y}} \right) + \text{ierfc} \left(\frac{2d}{\sqrt{y}} \right) \right] \quad (\text{C1})$$

where $d = D/H$, $y = 4\kappa\tau/H^2$ and $\kappa = \lambda/c$. The function f_m is given in Appendix B and ierfc denotes the integral of the complementary error function. The function $f_m(y)$ gives the vertical effects for an infinite caprock. The function f'_m replaces f_m in Formula B9 in Appendix B. We get the following expression for the recovery factor:

$$\epsilon = g_m \left(\frac{\kappa\tau}{R^2} \right) \cdot f'_m \left(\frac{D}{H}, \frac{4\kappa\tau}{H^2} \right) \quad (\text{C2})$$

Figure C1 shows $\epsilon(d)/\epsilon(\infty) = f'_m(d, y)/f_m(y)$ as a function of $1/\Lambda$ for several values of d .

References

- Bear, J., Dynamics of fluids in porous media, pp. 650-651, American Elsevier Publishing Company, Inc., 1972.
- Buscheck, T., Doughty, C. and Tsang, C.F., "Aquifer thermal energy storage - parameter study," Lawrence Berkeley Laboratory (in progress), 1981.
- Carslaw, H.S. and Jaeger, J.C., Conduction of Heat in Solids, 2nd ed., pp. 87-89, Oxford, Clarendon Press, 1959.
- Claesson, J., Efring, B., Hellström, G., "Temperature decline of a heated region in the ground," Dept. of Mathematical Physics, Lund University, Lund, Sweden, Lund-MPh-80122, 1980.
- Fabris, H. and Gringarten, A.C., "Etudes expérimentales de stockage et de transfert de chaleur en aquifère." RS-598 in Summary of the Principal Scientific and Technical Results of the National Geological Service for 1977, Supplement to the Bulletin of the BRGM, National Geological Service, Orléans, France, 1977.
- Fabris, H., Gringarten, A.C., Landel, P.A., Noyer, M.L. and Sauty, J.P., "Etude des possibilités du stockage d'eau chaude en aquifère profond," 1er rapport d'avancement. Rapport BRGM 77 SGN 658 HYD, 1977.
- Hellström, G. and Claesson, J., "Heat losses and temperature fields for heat storage aquifers. A computational model with a simplified water flow," in Theoretical Analysis and Computer Simulation of Solid-Fluid Heat Storage Systems in the Ground. Extraction of Earth Heat. Interim Report Part II, Department of Mathematical Physics and Building Science, Lund Institute of Technology, Lund, Sweden, 1978.
- Hellström, G., Tsang, C.F. and Claesson, J., "Heat storage in aquifers. Buoyancy flow and thermal stratification problems." Department of Mathematical Physics, Lund Institute of Technology, Lund, Sweden, 1979.
- Iris, P., "Expérimentation de stockage des chaleur intersaisonnier en nappe phréatique Campuget (Gard) 1977-1978." Ecoles des Mines de Paris Centre d'Informatique Géologique, Fontainebleau, 1979.
- Lawrence Berkeley Laboratory, "Proceedings of Thermal Energy Storage in Aquifers Workshop," held May 10-12, 1978 at Lawrence Berkeley Laboratory, Berkeley, California, LBL-8431, 1978.
- Mathey, B., "Development and resorption of a thermal disturbance in a phreatic aquifer with natural convection." Journal of Hydrology, v. 34, pp. 315-333, 1977.
- Menjöz, A. and Sauty, J.P., "Stockage de calories en aquifère par convection forcée a partir d'un puits unique," presented at 7ème Symposium International sur les Transferts de Chaleur et de Mass en Milieu Poreux - Toulouse, France, August 26-28, 1980.

Molz, F.J., Parr, A.P., Andersen, P.F., Lucido, V.D., and Warman, J.C., "Thermal energy storage in a confined aquifer. Experimental Results". Water Resources Research, in press.

Reddell, D.L., Davison, R.R. and Harris, W.B., "Thermal storage of cold water in groundwater aquifers for cooling purposes." In Proceedings of Thermal Energy Storage in Aquifers Workshop, Lawrence Berkeley Laboratory, Berkeley, California, LBL-8431, pp. 51-55, 1978.

Sauty, J. P., Gringarten, A. C., Menjoz, A. and Landel, P. A., "Sensible energy storage in aquifers: 1-Theoretical Study," Bureau de Recherches Geologiques et Minieres, Service Geologique National, Orleans, France, 1980.

Scheidegger, A., The Physics of Flow through Porous Media, 2nd rev. edition, pp. 256-259, MacMillan, 1960.

Tsang, C.F., Buscheck, T. and Doughty, C., "ATES - a numerical simulation of Auburn University field experiments," Lawrence Berkeley Laboratory, Berkeley, California, LBL-10210, 1980.

Tsang, C.F., Buscheck, T., Mangold, D. and Lippmann, M., "Mathematical modeling of thermal energy storage in aquifers," in Proceedings of Thermal Energy Storage in Aquifers Workshop, Lawrence Berkeley Laboratory, Berkeley, California, LBL-8431, pp. 37-45, 1978.

Tsang, C.F., Hopkins, D. and Hellström, G., "Aquifer thermal energy storage - a survey," Lawrence Berkeley Laboratory, Berkeley, California, LBL-10441, 1980.

Tsang, C.F., Lippmann, M.J., Goranson, C.B. and Witherspoon, P.A., "Numerical modeling of cyclic storage of hot water in aquifers," Lawrence Berkeley Laboratory, Berkeley, California, LBL-5929, 1977.

Tsang, C.F. and Witherspoon, P.A., "An investigation of screening geothermal production wells from effects of reinjection." In Kruger, P., and Ramey, J.J., eds., Geothermal reservoir engineering. Stanford, Stanford Geothermal Program Rpt. SGP-TR-12, pp. 62-64, 1975.

Whitehead, W.R. and Langhete, E.J., "Use of bounding wells to counteract the effects of preexisting groundwater movement," Water Resources Res. v. 14, no. 2, pp. 273-280, 1978.

Yokoyama, T., Unemiya, H., Teraoka, T., Watanabe, H., Katsuragi, K. and Kasamaru, K., "Seasonal regeneration through underground strata." In Proceedings of Thermal Energy Storage in Aquifers Workshop, Lawrence Berkeley Laboratory, Berkeley, California, LBL-8431, pp. 94-106, 1978.

TABLE 1. PARAMETERS USED WITH THE STEADY FLOW MODEL GRAPHS TO PREDICT RECOVERY FACTOR

	Site Specific Parameters									Engineered Parameters					Intermediate Derived Parameters			Dimensionless Groups				Recovery Factors			
	H (m)	D (m)	C _a (10 ⁶ J/m ³ K)	C _c	C _w	λ _a (J/msK)	λ _c	d ₁₁ (m)	d ₁ (m)	v _w (m ³)	t _i	t _s	t _p (days)	t _r	R (m)	τ (days)	λ̄ (J/msk)	Pe	Λ	λ̄ _a /λ _c	d	Predicted		Observed	
																						1st	5th	1st	4th
REFERENCE CASE	50	∞	2.5	2.0	4.1	2.5	2.5	0.	0.	60,000	90	90	90	90	25	180	2.5	39.6	396.4	1	∞	.77	.85		
FIELD EXPERIMENTS																									
Auburn	21	9	2.4	2.6	4.1	2.29	2.56	-	-	55,000	79	50	41	-	37.7	110	*4.58	78.4	80.3	2	.4	.71	.79	.66	-
Modified Auburn**	16	"	"	"	"	"	"	"	"	"	"	"	"	"	43	"	"	101.9	46.6	"	.5	.68	.77	"	-
Bonnaud	2.5	4	2.6	2.6	4.1	2.5	2.5	1	-	490	6	0	6	0	10	6	32.6	15.4	25.2	13	1.6	.50	.64	-	.677

*λ_a ascertained from independent numerical modeling work (Tsang et al., 1980; Buscheck et al., 1981)

** R determined from temperature observations, H derived by conserving volume.

$$R = \sqrt{\frac{C_w V}{C_a \pi H}}$$

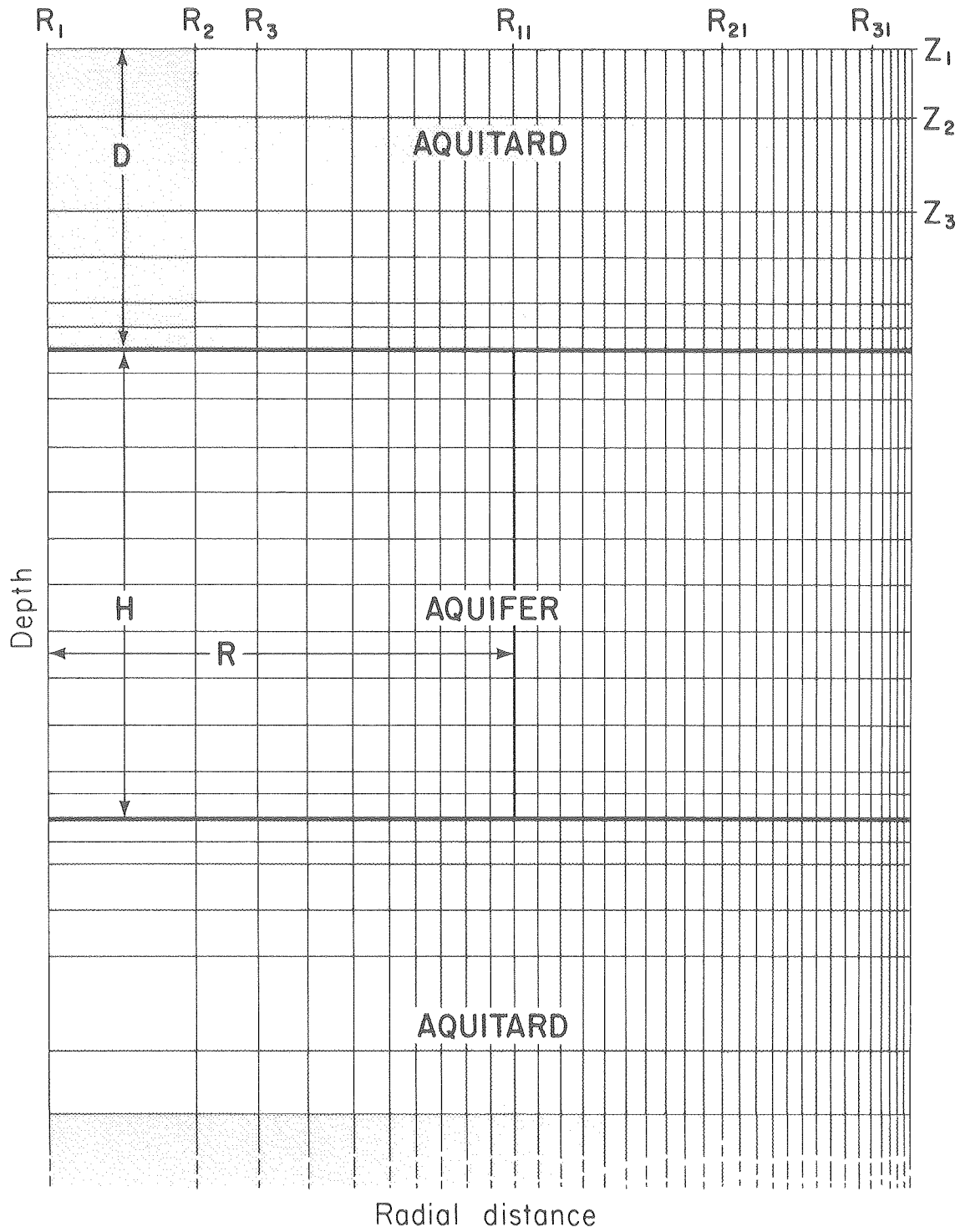
$$\tau = \frac{1}{2}(t_i + t_p) + t_s$$

$$\bar{\lambda}_a = \lambda_a + \frac{.3d_{11}RC_a}{(\tau/2)}$$

$$Pe = \frac{C_a R^2}{2\lambda_a (\tau/2)}$$

$$\Lambda = \frac{C_a^2 H^2}{C_c \lambda_c (\tau/2)}$$

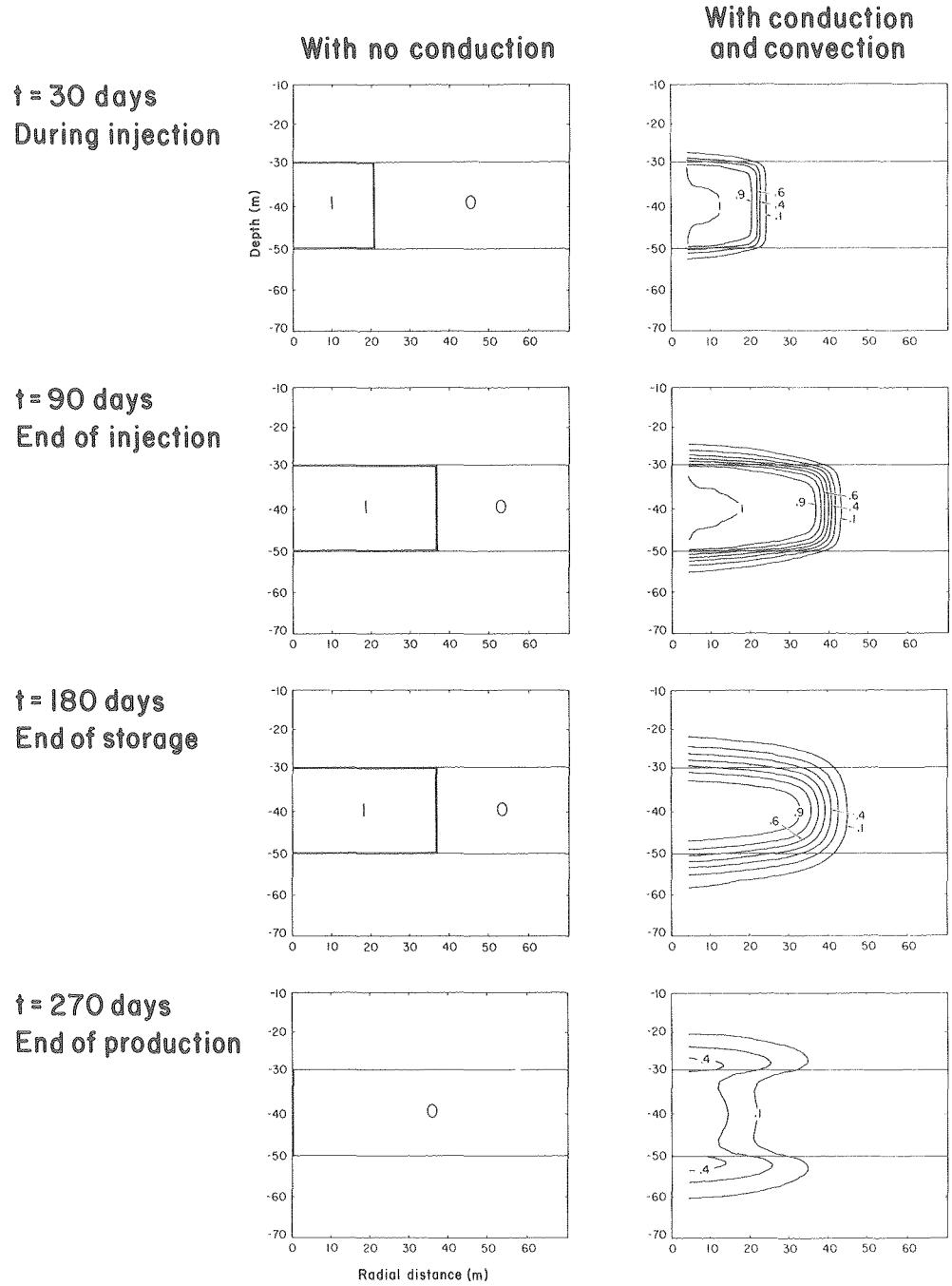
$$d = \frac{D}{H}$$



XBL 807-1388

1. Scale drawing of part of the equal volume mesh. The mesh may extend further vertically than is shown to simulate infinitely thick confining layers.

TEMPERATURE FIELDS
SIMULATED BY STEADY FLOW MODEL

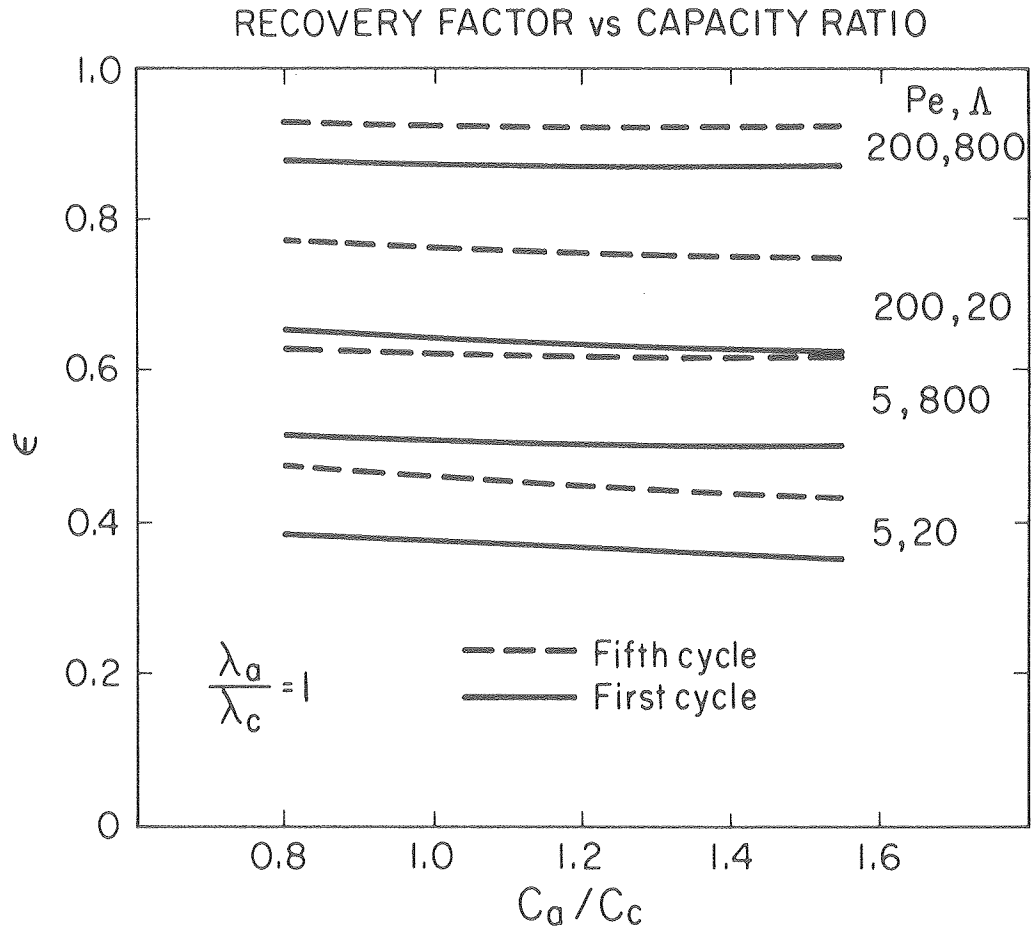


$\epsilon = 1$

$\epsilon < 1$

XBL 807-1386

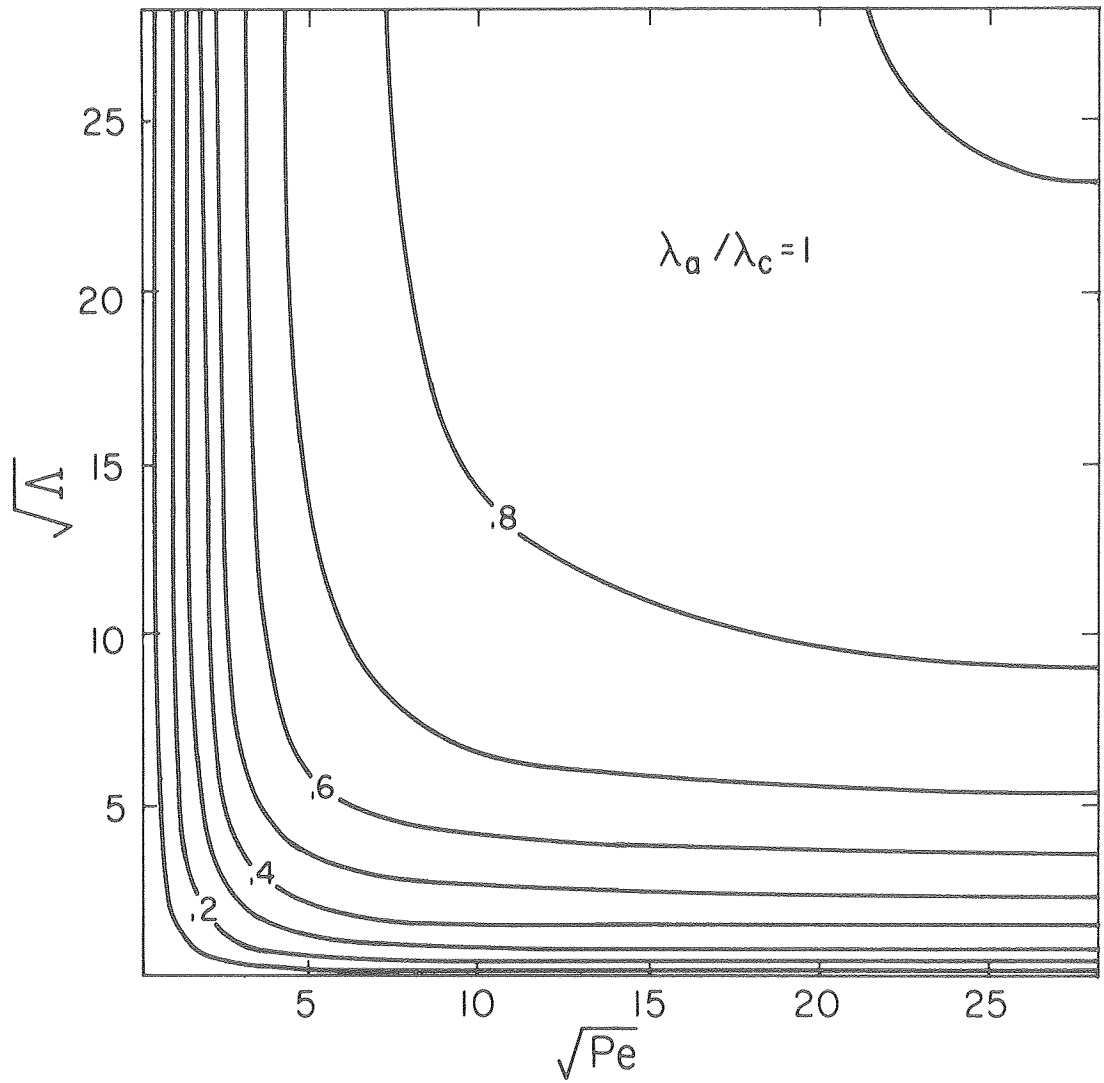
- Temperature distributions at various times during the first cycle generated by the SFM with and without conduction.



XBL 8012-6515

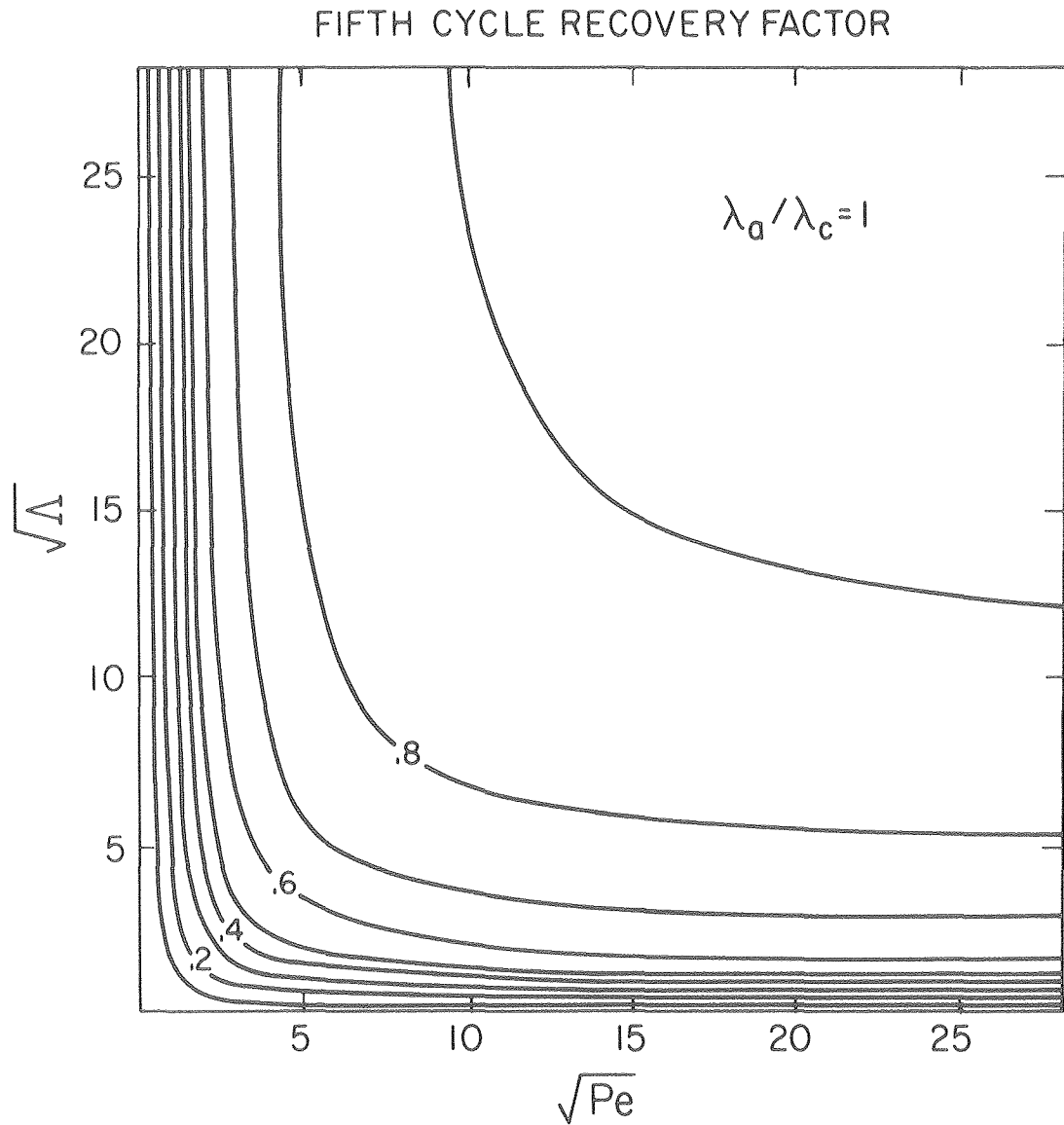
3. First and fifth cycle recovery factors as a function of heat capacity ratio C_a/C_c , for various values of Pe and Λ .

FIRST CYCLE RECOVERY FACTOR



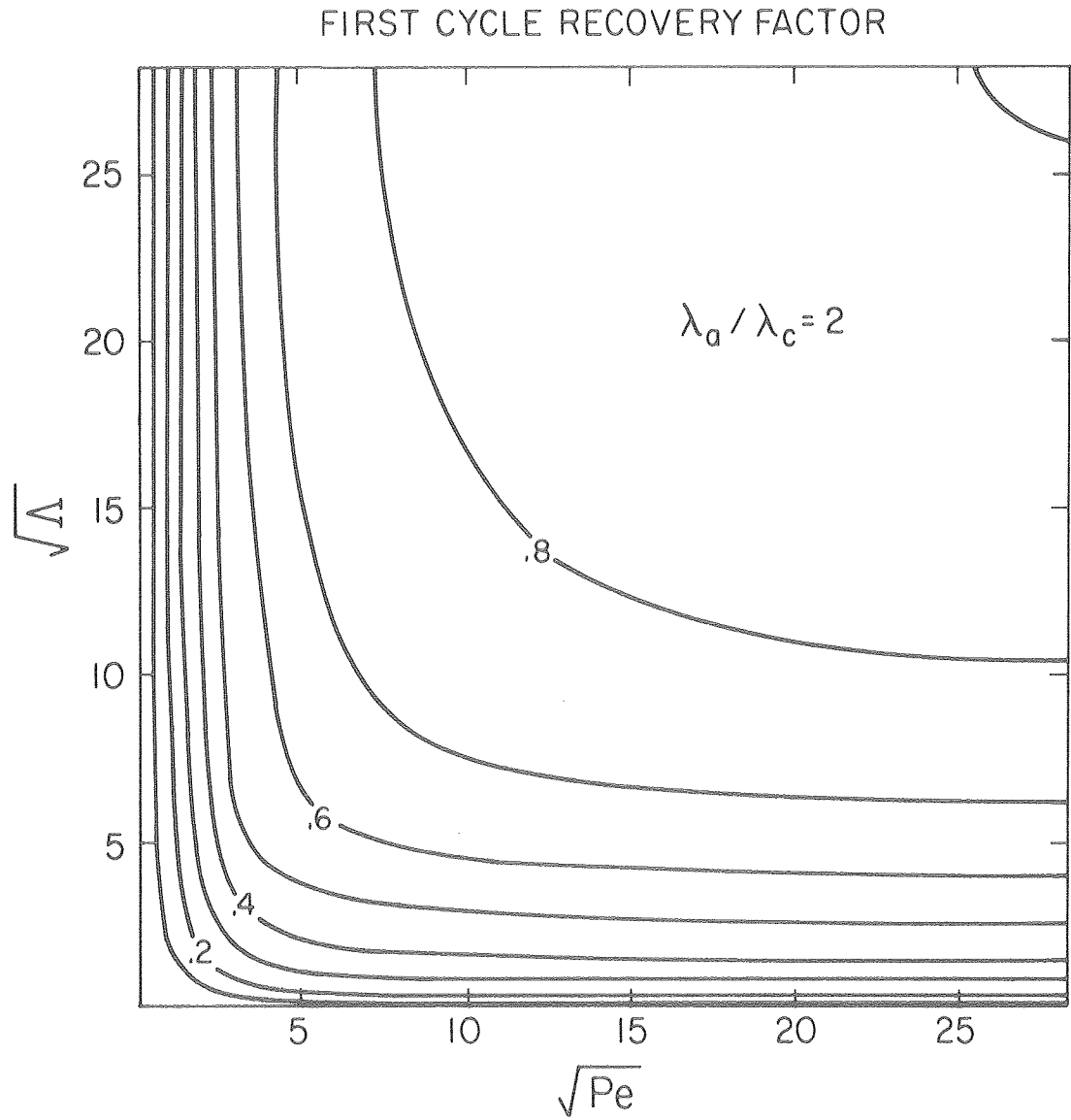
XBL8012-6516

4. Recovery factor as a function of \sqrt{Pe} and $\sqrt{\Lambda}$, for the first and fifth cycles, when $\lambda_a/\lambda_c = 1, 2,$ and 10 .



XBL 8012-6517

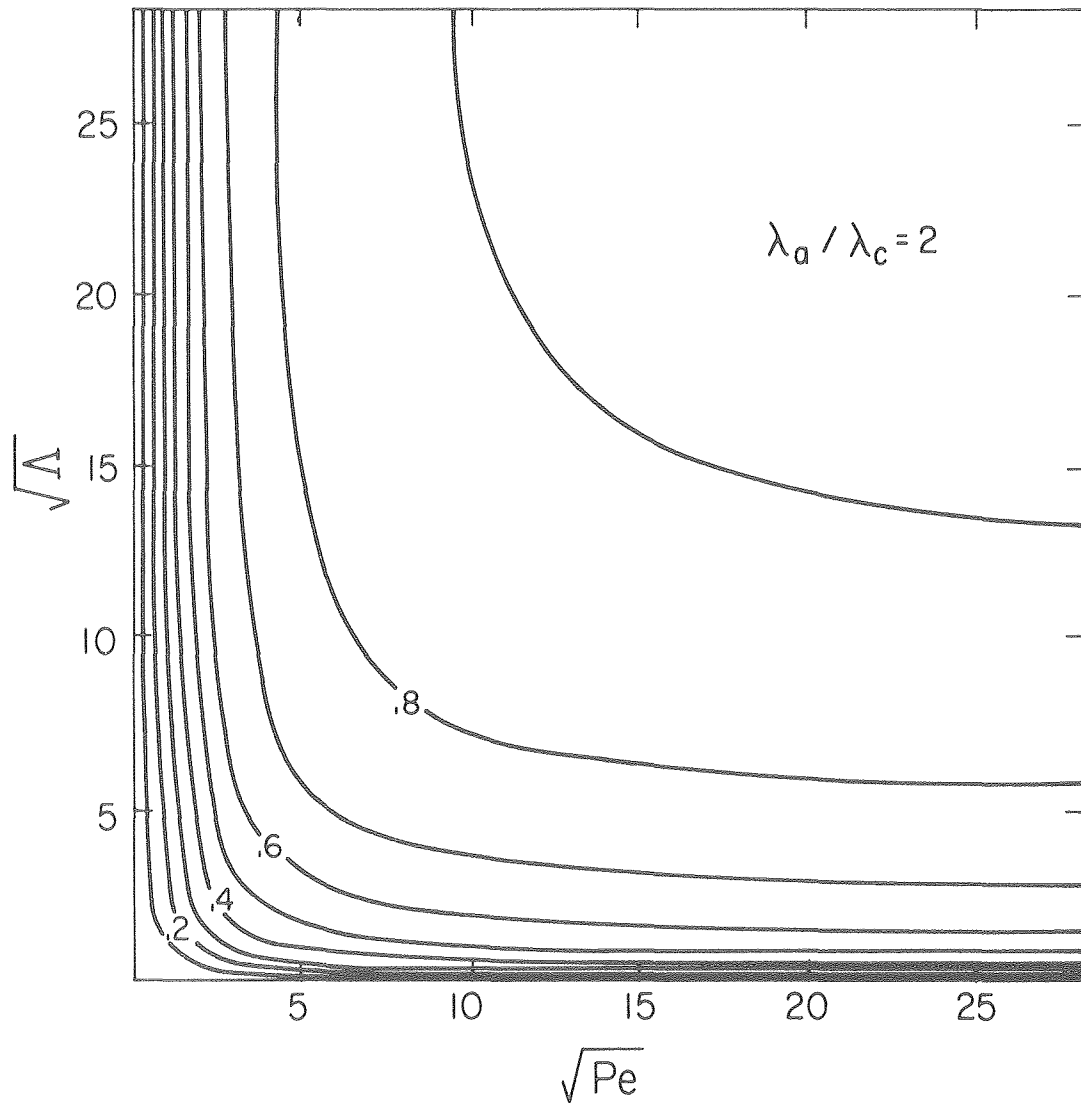
5. Recovery factor as a function of \sqrt{Pe} and $\sqrt{\Lambda}$, for the first and fifth cycles, when $\lambda_a/\lambda_c = 1, 2,$ and 10 .



XBL 8012-6518

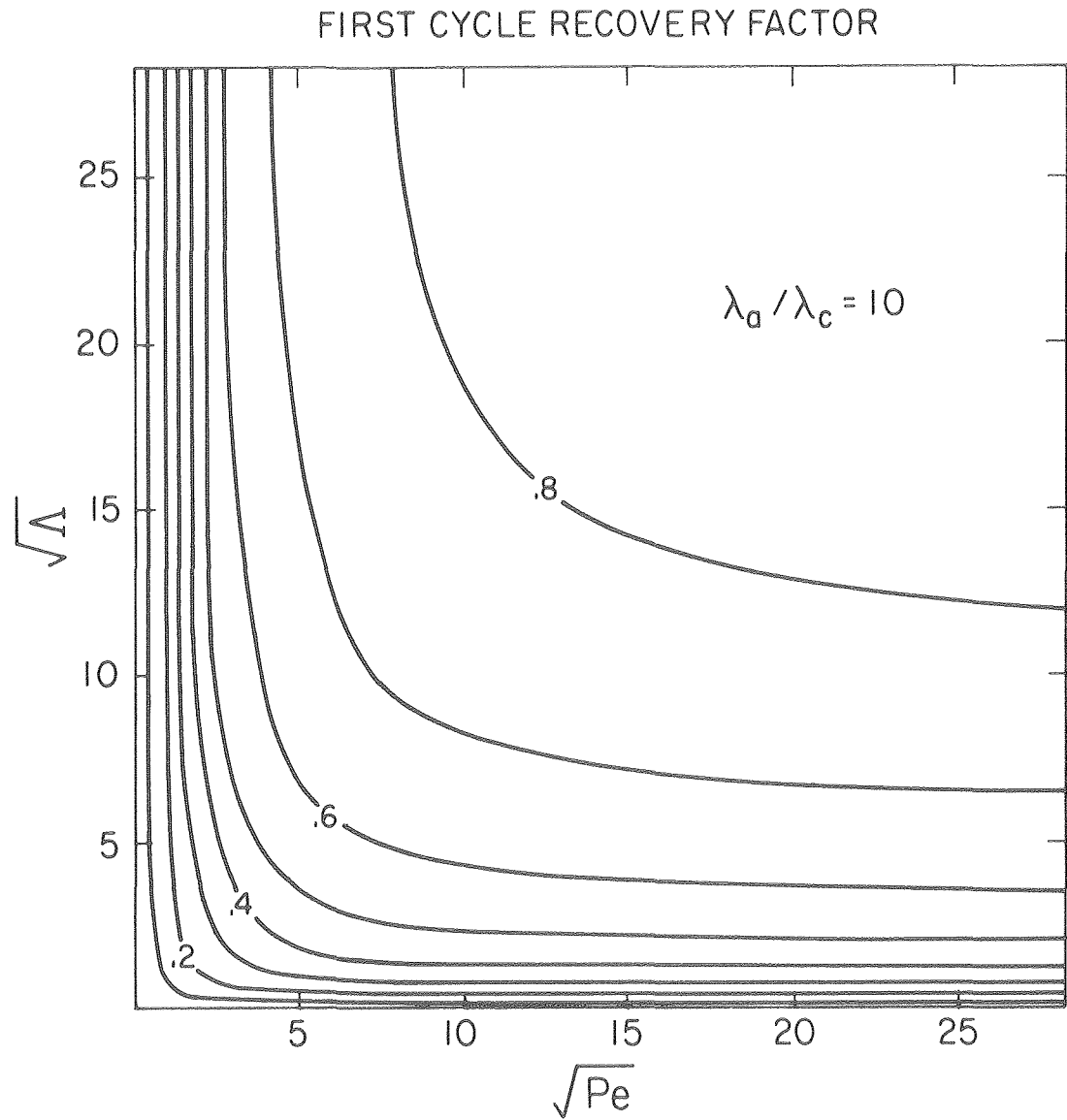
6. Recovery factor as a function of \sqrt{Pe} and $\sqrt{\Lambda}$, for the first and fifth cycles, when $\lambda_a / \lambda_c = 1, 2,$ and 10 .

FIFTH CYCLE RECOVERY FACTOR

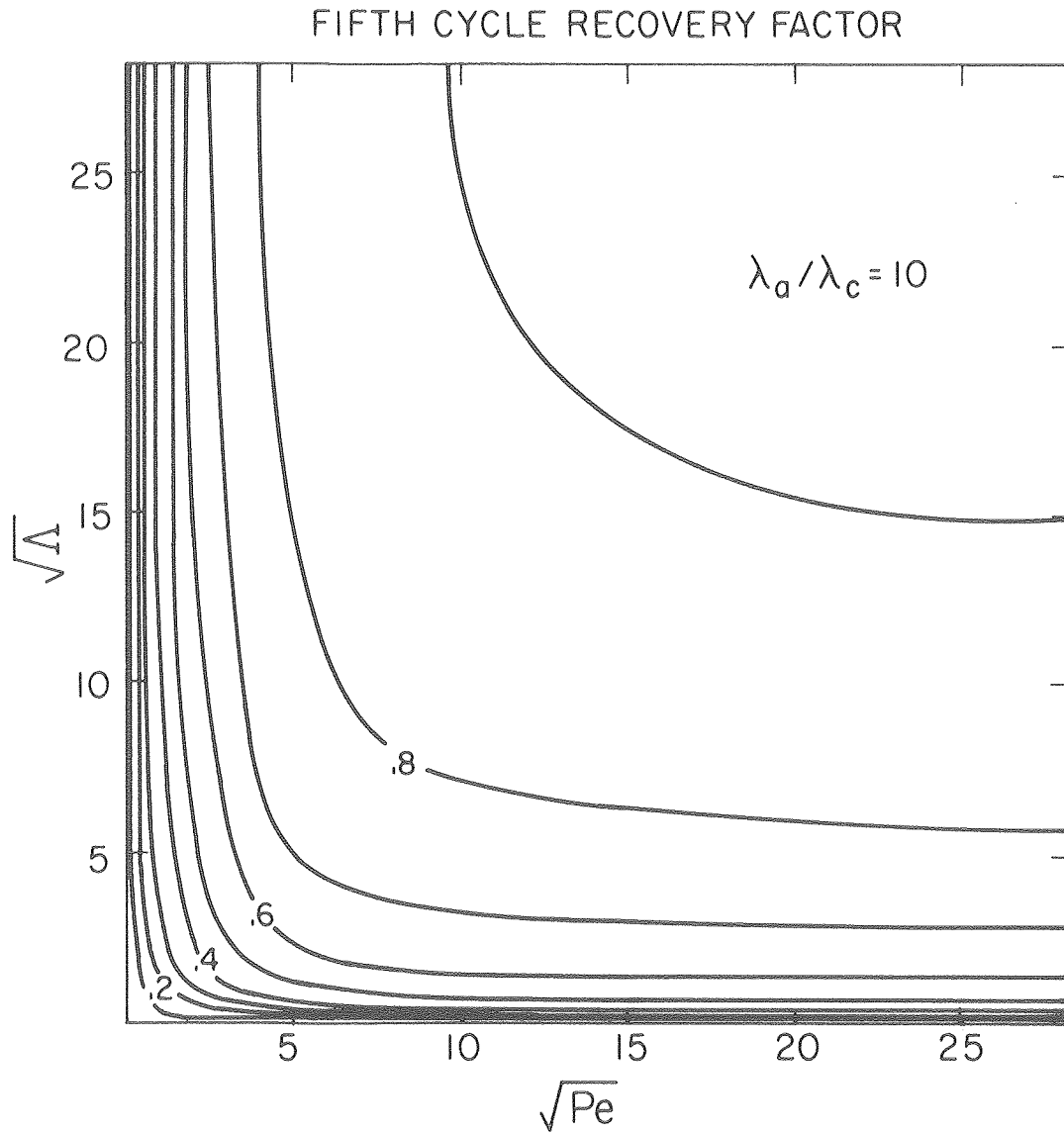


XBL8012-6519

7. Recovery factor as a function of \sqrt{Pe} and $\sqrt{\Lambda}$, for the first and fifth cycles, when $\lambda_a/\lambda_c = 1, 2,$ and 10 .

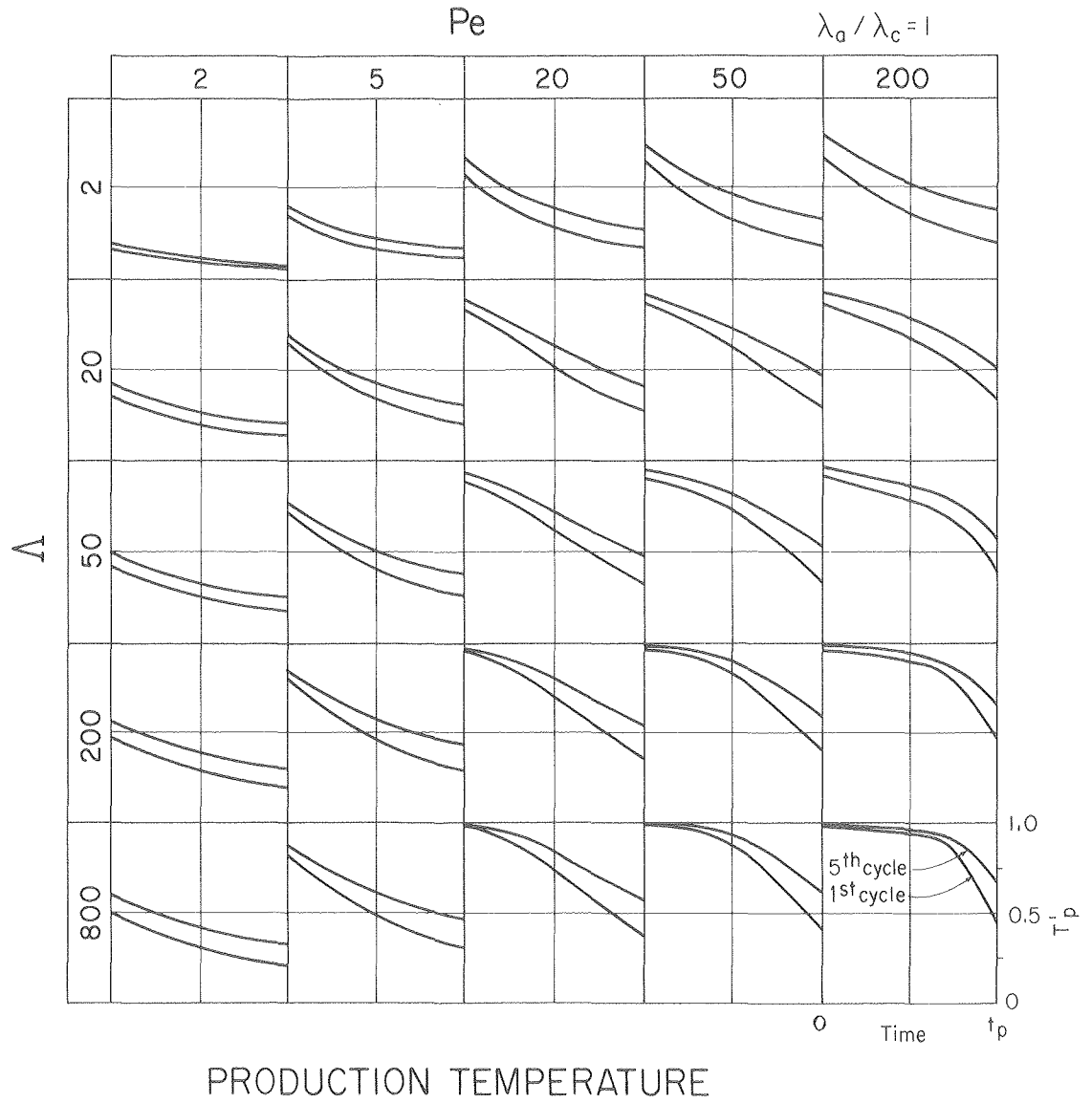


8. Recovery factor as a function of \sqrt{Pe} and $\sqrt{\Lambda}$, for the first and fifth cycles, when $\lambda_a / \lambda_c = 1, 2,$ and 10 .

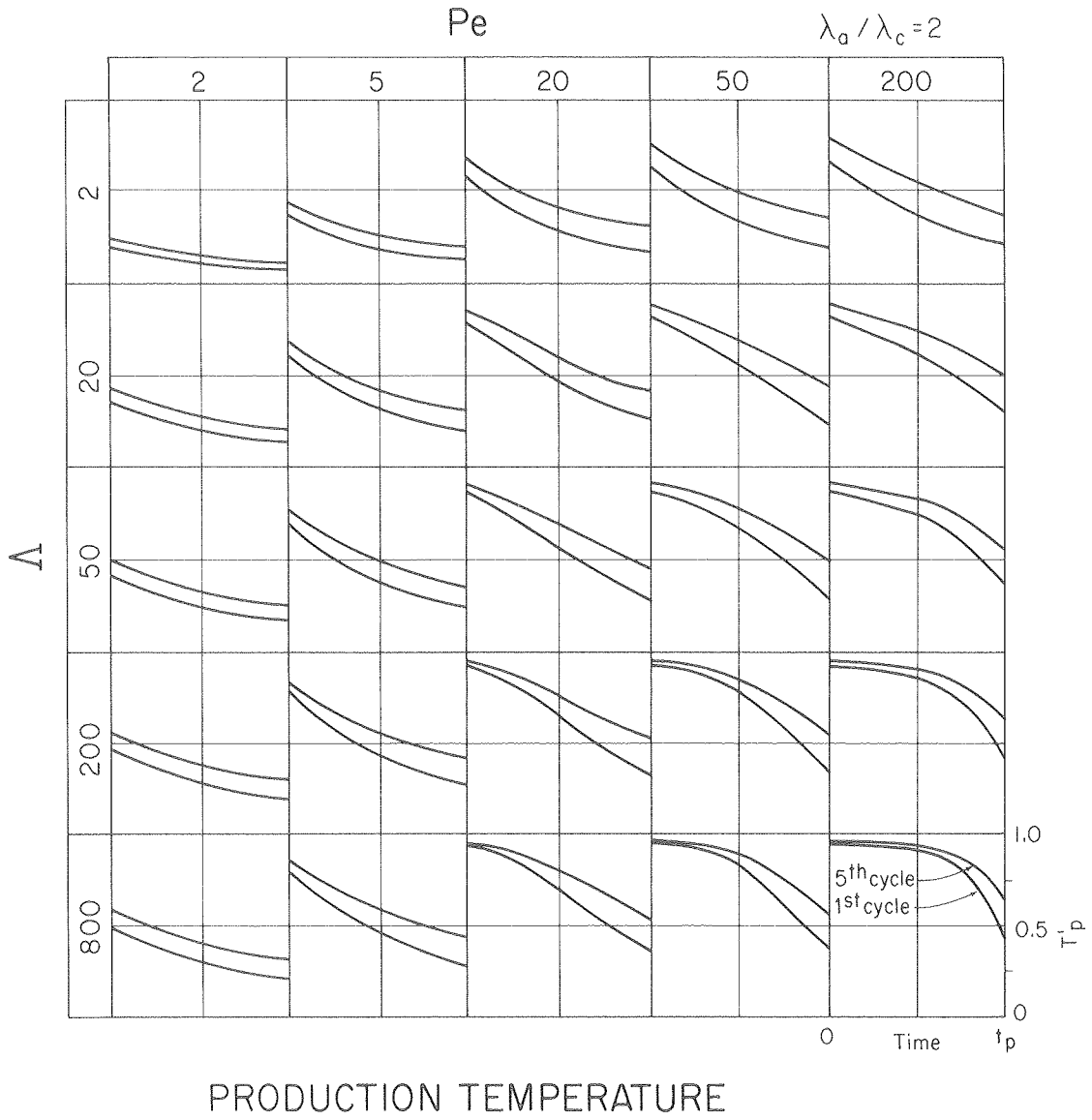


XBL 8012-6521

9. Recovery factor as a function of \sqrt{Pe} and $\sqrt{\Lambda}$, for the first and fifth cycles, when $\lambda_a/\lambda_c = 1, 2, \text{ and } 10$.

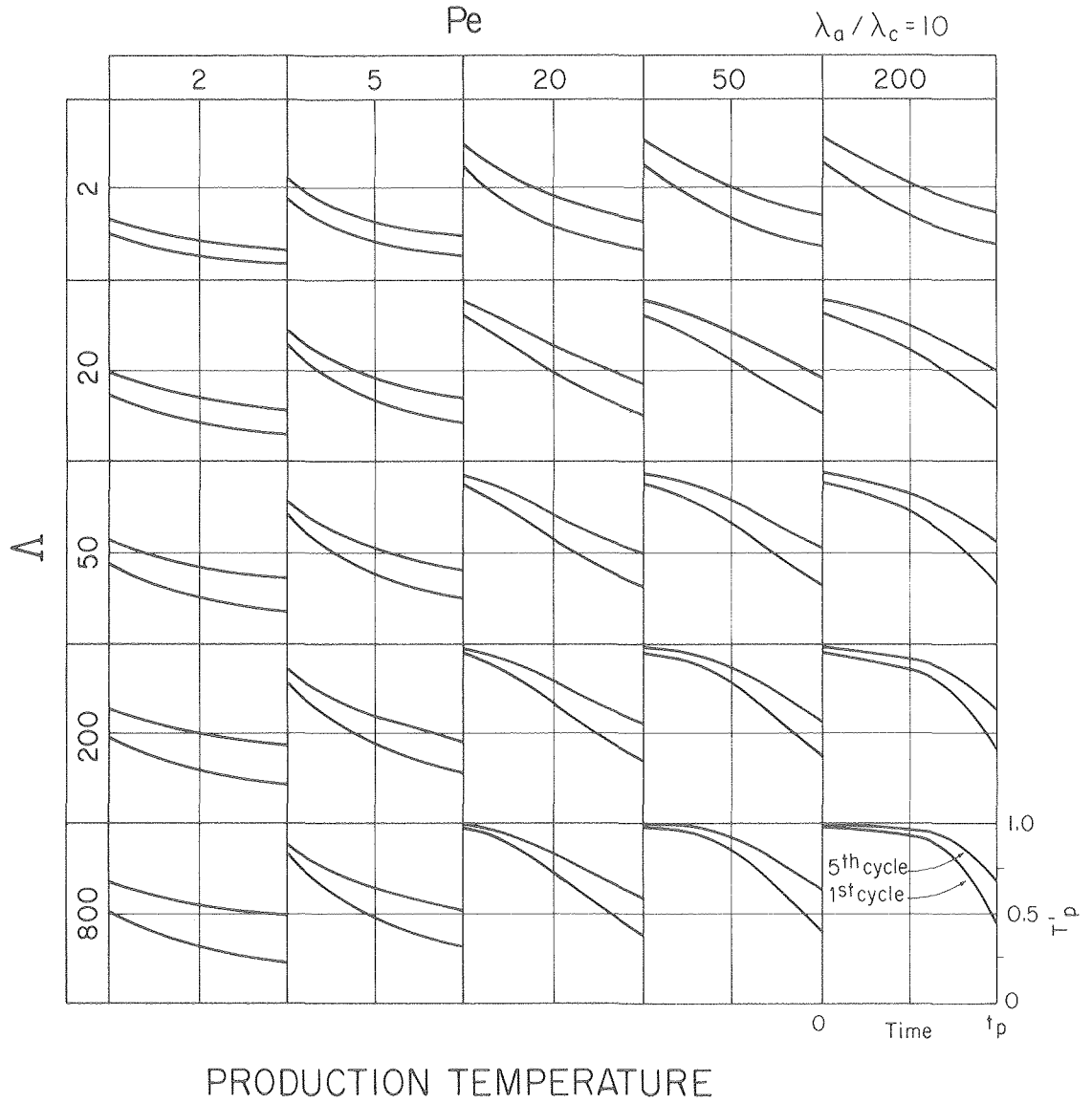


10. First and fifth cycle production temperatures versus time for a range of Pe and Λ when $\lambda_a/\lambda_c = 1, 2,$ and 10 .



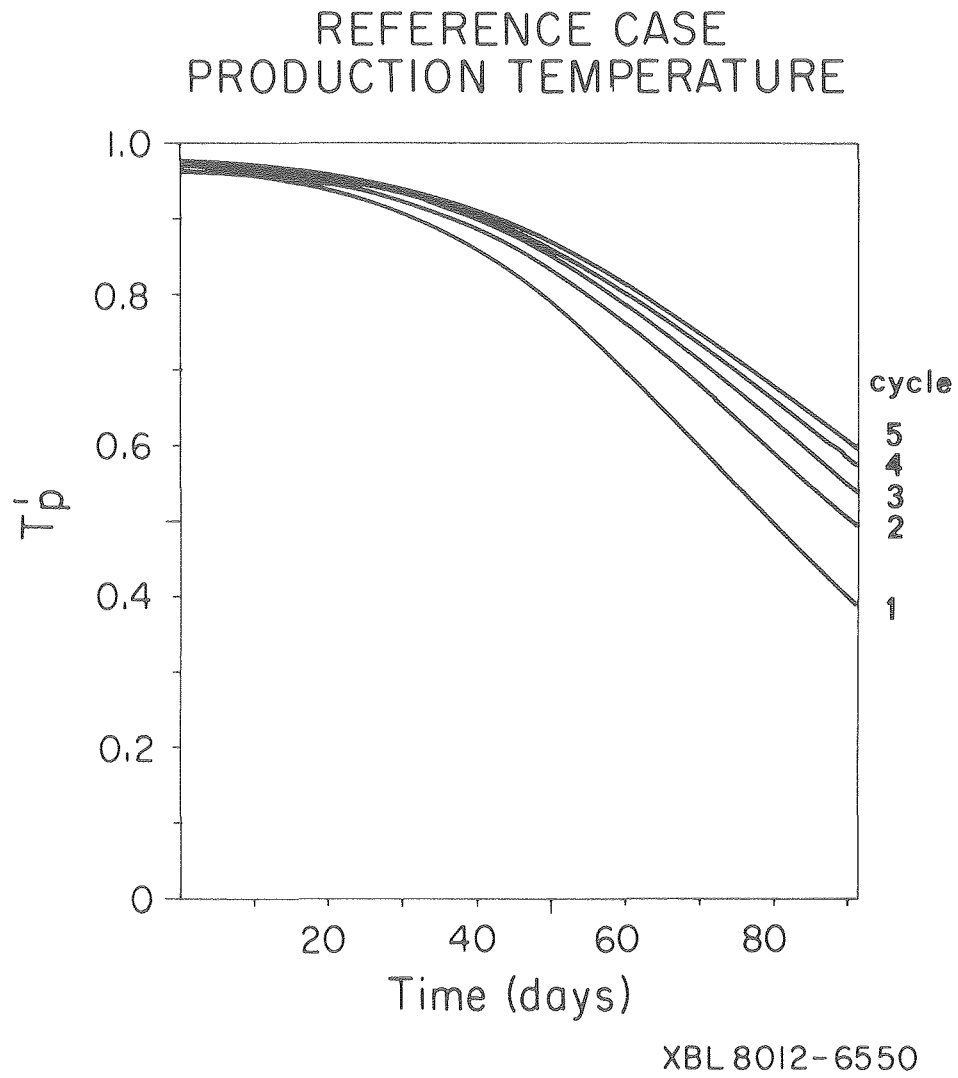
XBL8012-6582E

11. First and fifth cycle production temperatures versus time for a range of Pe and Λ when $\lambda_a / \lambda_c = 1, 2,$ and 10 .



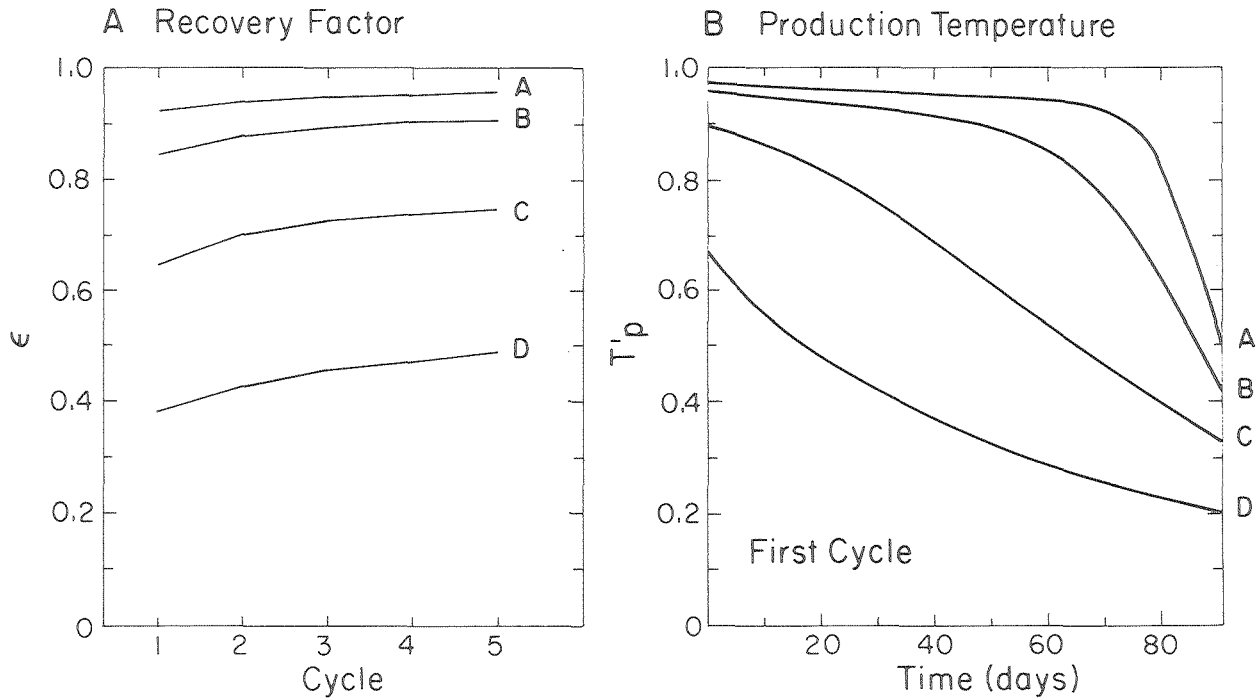
XBL8012-6582D

12. First and fifth cycle production temperatures versus time for a range of Pe and Λ when $\lambda_a / \lambda_c = 1, 2,$ and 10 .



13. Production temperature versus time for the first five cycles of the reference case.

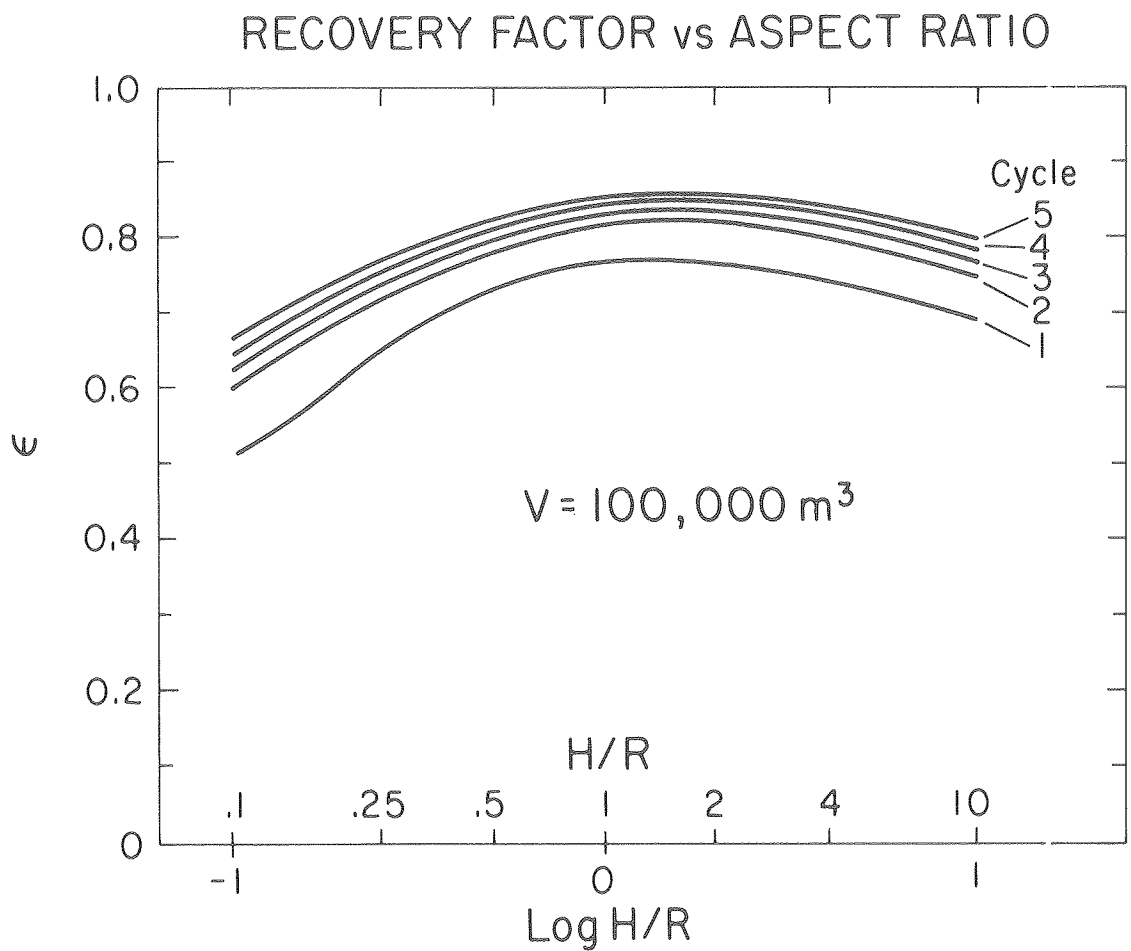
THERMAL VOLUME VARIATION



	R(m)	H(m)	Pe	Λ	V(m ³)	V _w (m ³)
A	100	100	634	1585	3,100,000	1,900,000
B	50	50	159	396	390,000	240,000
C	20	20	25.4	63.4	25,000	15,000
D	10	10	6.3	15.8	3,100	1,900

XBL 8012-6551

14. Recovery factor for different thermal volumes for the first five cycles and first cycle production temperature versus time for different thermal volumes.

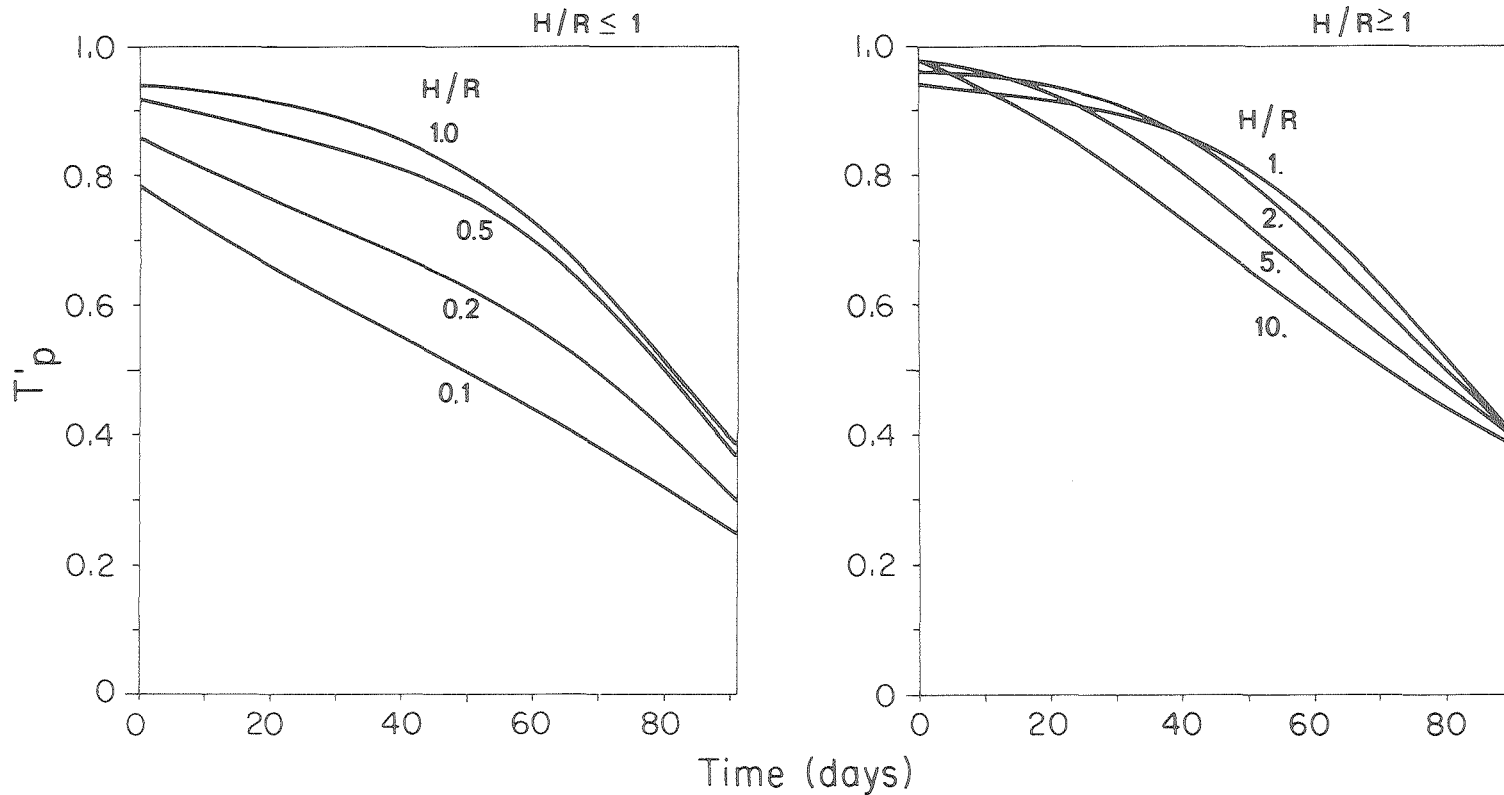


XBL 8012-6552

15. Recovery factor as a function of aspect ratio for the first five cycles.

FIRST CYCLE PRODUCTION TEMPERATURES FOR VARIOUS ASPECT RATIOS

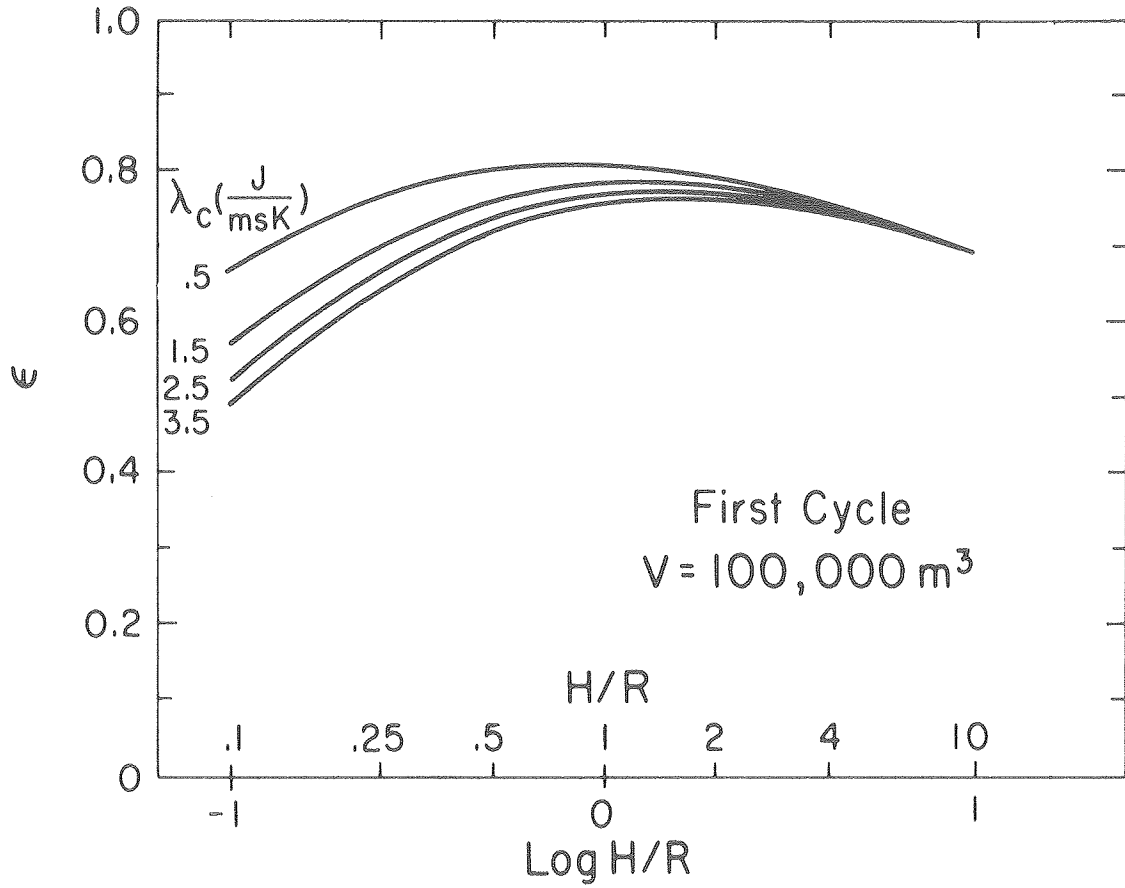
$V = 100,000 \text{ m}^3$



XBL 8012-6553

16. First cycle production temperature versus time for different aspect ratios.

RECOVERY FACTOR vs ASPECT RATIO
Aquitard Conductivity Variation

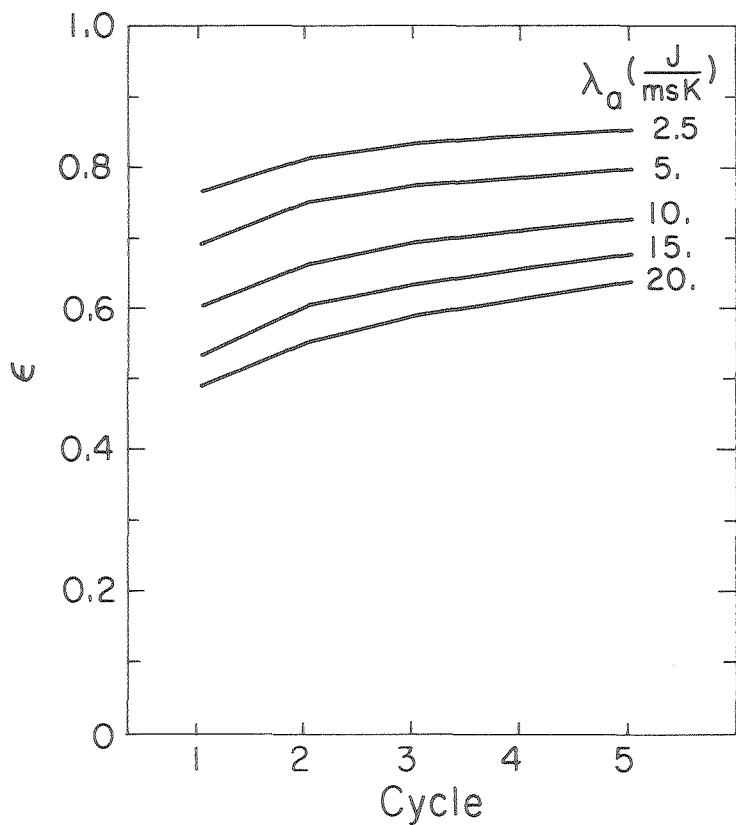


XBL 8012-6555

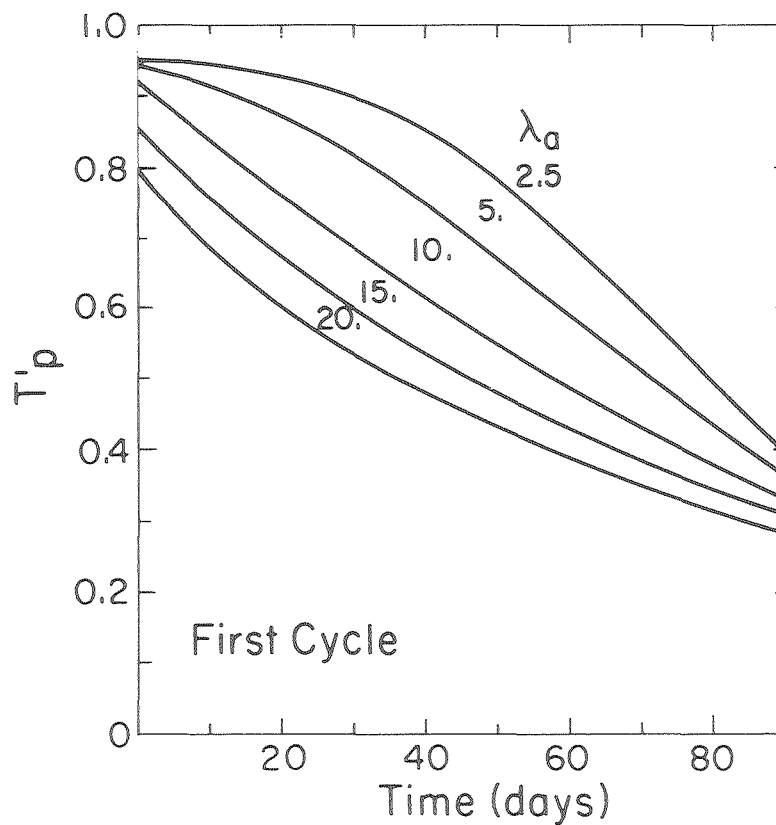
17. First cycle recovery factor as a function of aspect ratio for different values of aquitard thermal conductivity.

AQUIFER THERMAL CONDUCTIVITY VARIATION

A Recovery Factor



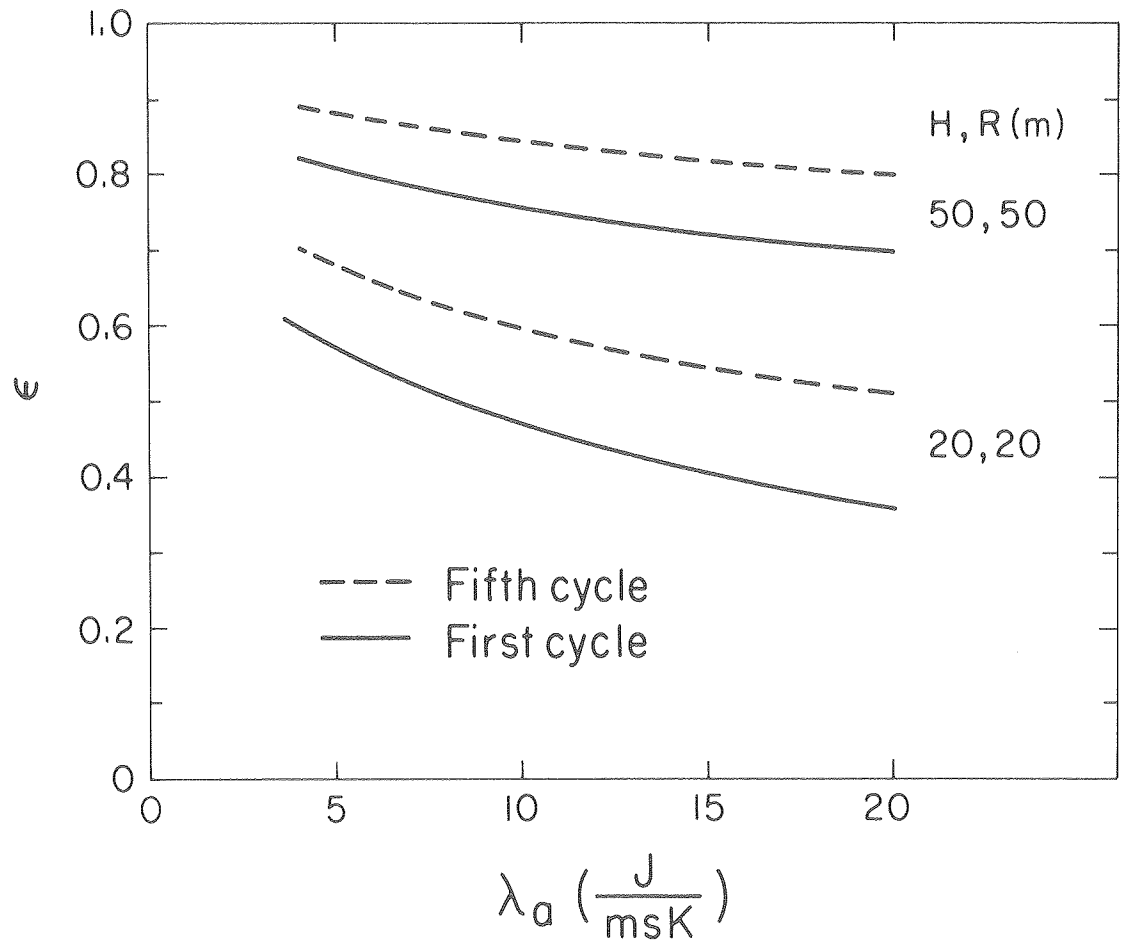
B Production Temperature



XBL 8012-13815

18. Recovery factor for different values of the aquifer thermal conductivity for the first five cycles and first cycle production temperature versus time for different values of the aquifer thermal conductivity.

RECOVERY FACTOR vs AQUIFER CONDUCTIVITY

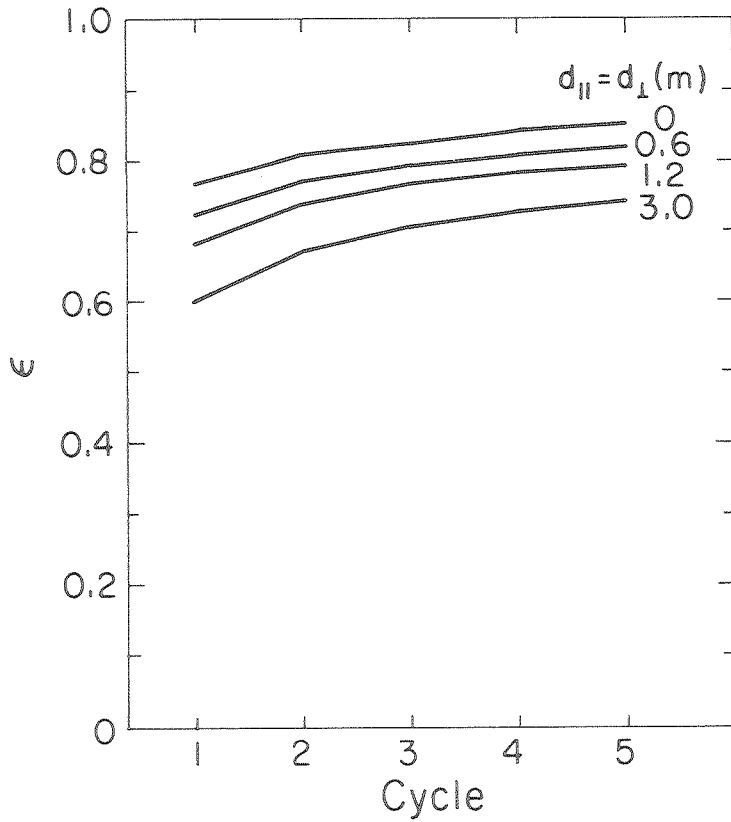


XBL 8012 - 6557

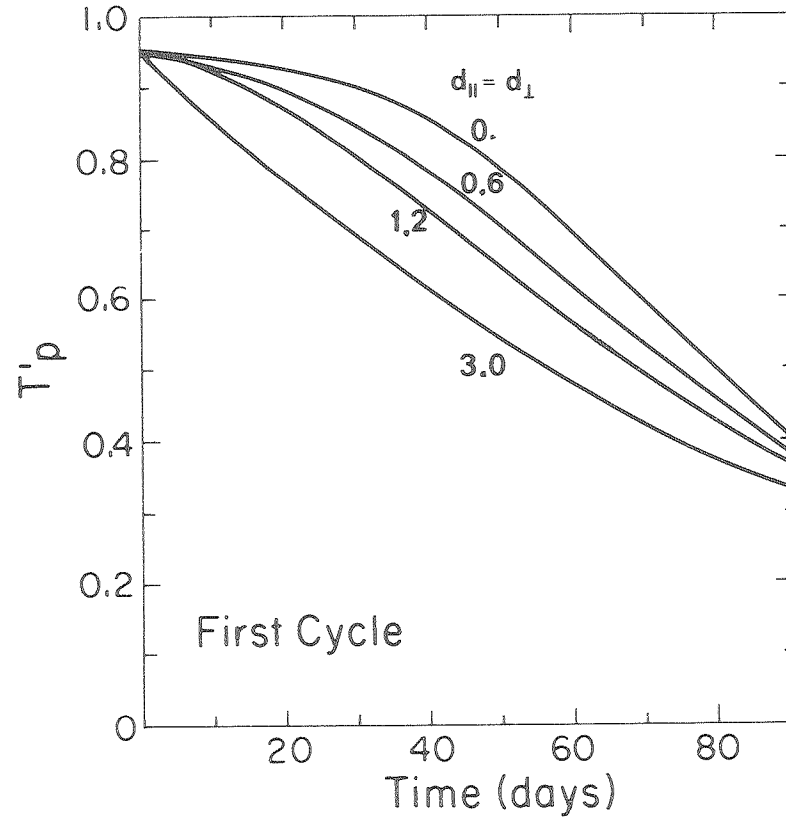
19. First and fifth cycle recovery factors as a function of the aquifer thermal conductivity.

DISPERSION LENGTH VARIATION

A Recovery Factor



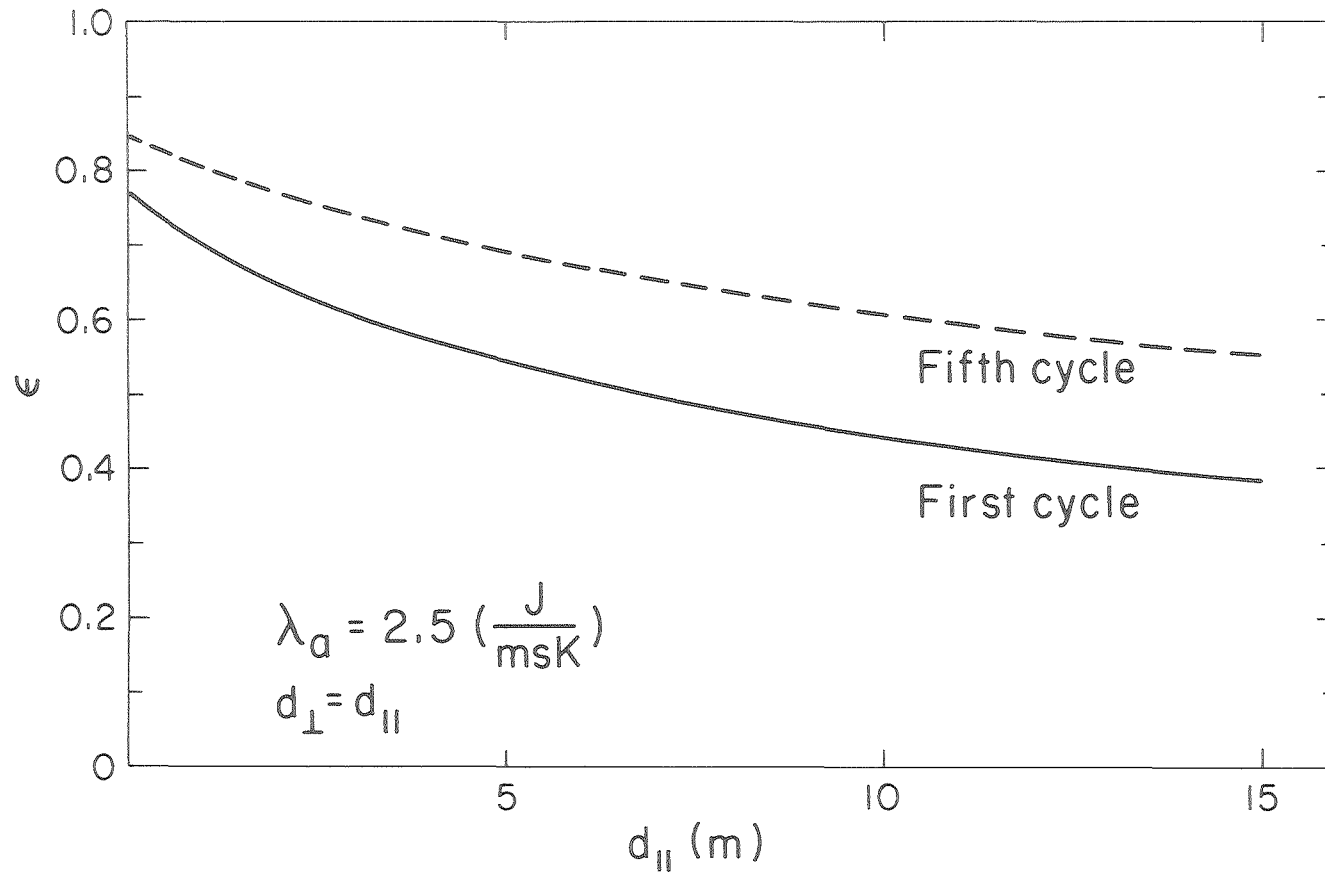
B Production Temperature



XBL 8012-6558

20. Recovery factor for different values of the dispersion length for the first five cycles and first cycle production temperature versus time for different values of the dispersion length.

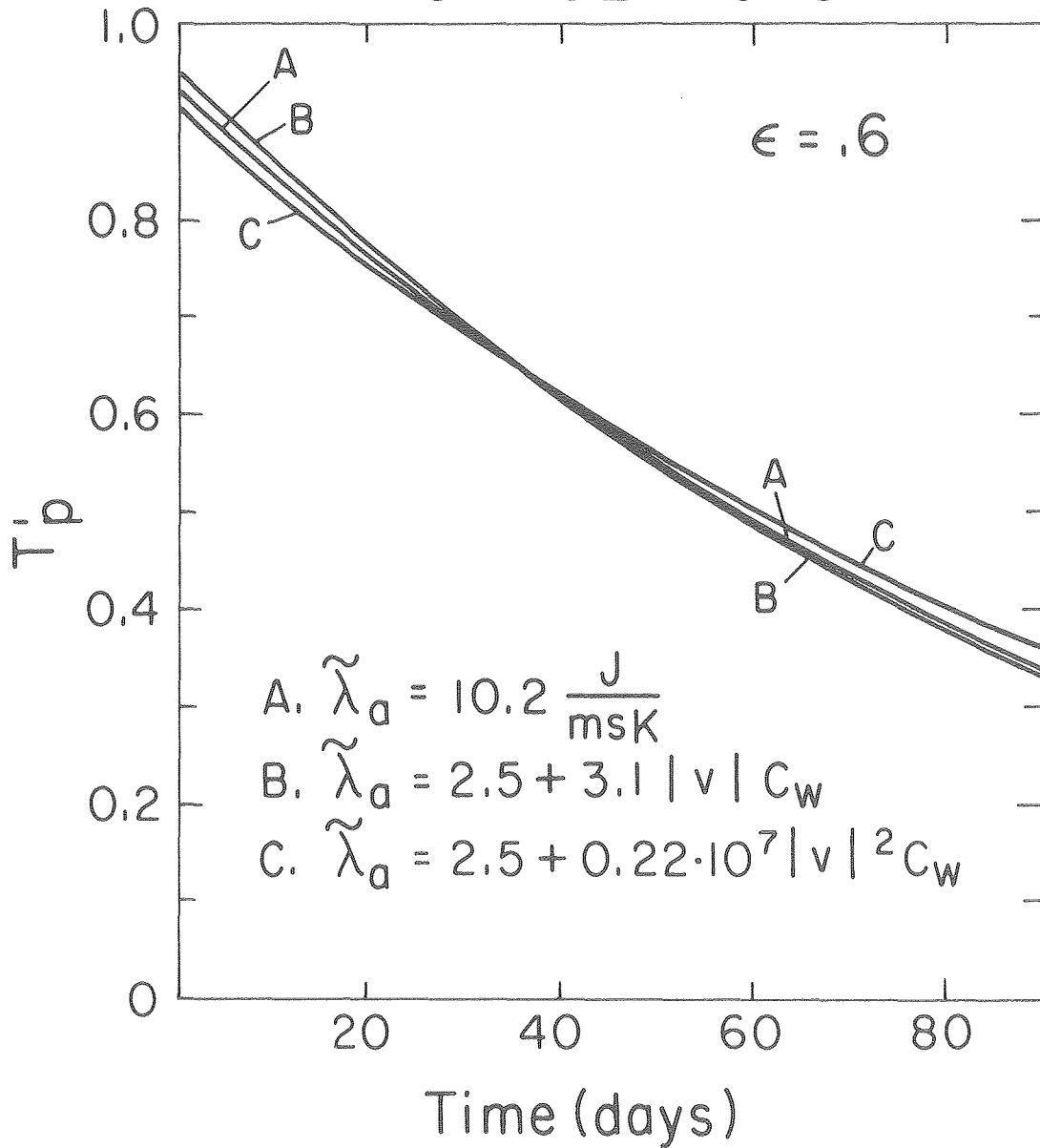
RECOVERY FACTOR vs DISPERSION LENGTH



XBL 8012-6559

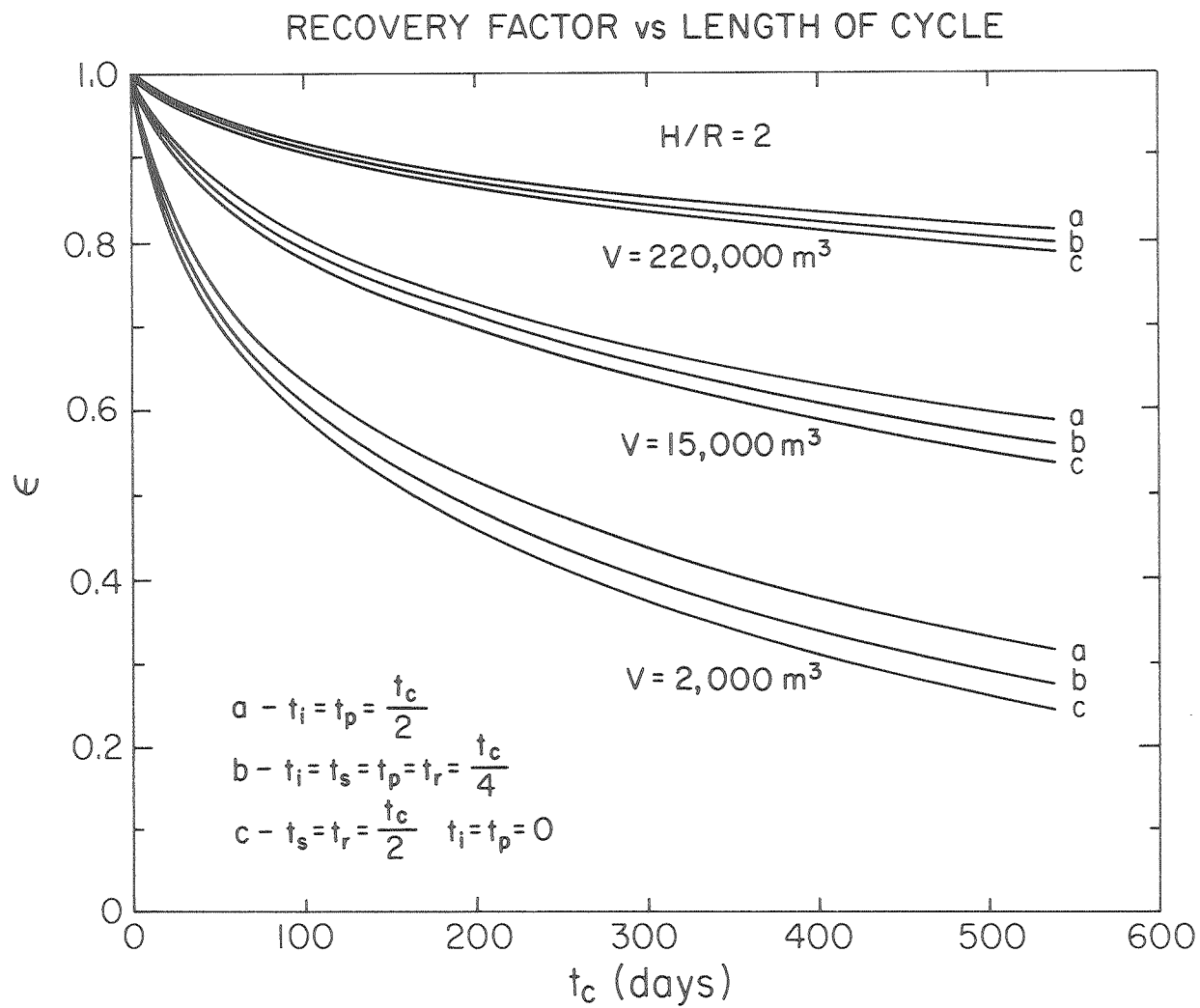
21. First and fifth cycle recovery factors as a function of dispersion length.

PRODUCTION TEMPERATURES FOR VARIOUS DISPERSION FORMULATIONS



XBL 8012-6560

22. First cycle production temperature versus time for different dispersion formulations.

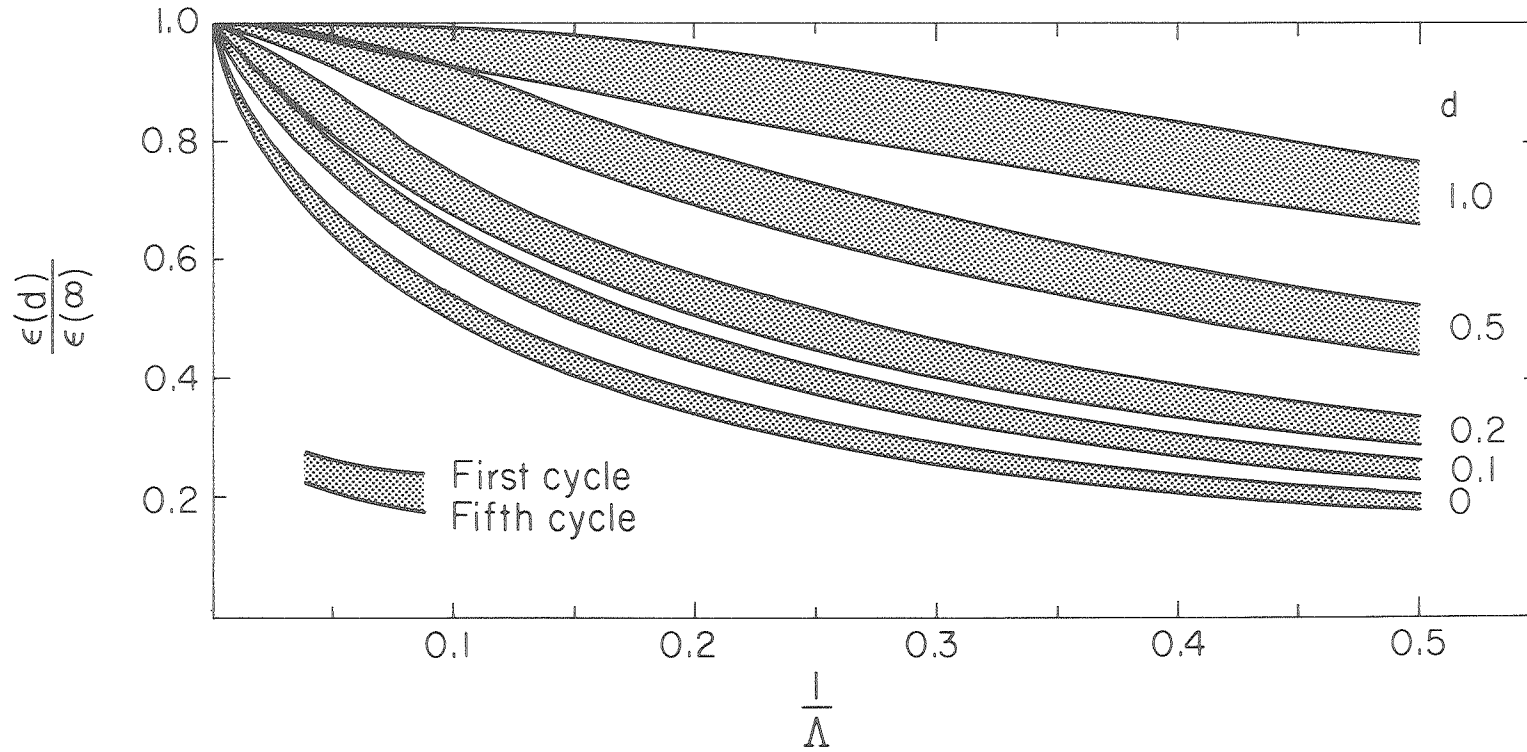


XBL807-1385

23. First cycle recovery factor versus cycle length for several injection-storage-production-rest schedules, for three thermal volumes.

FINITE THICKNESS CAPROCK EFFECT ON RECOVERY FACTOR

$$\lambda_a / \lambda_c = 1$$

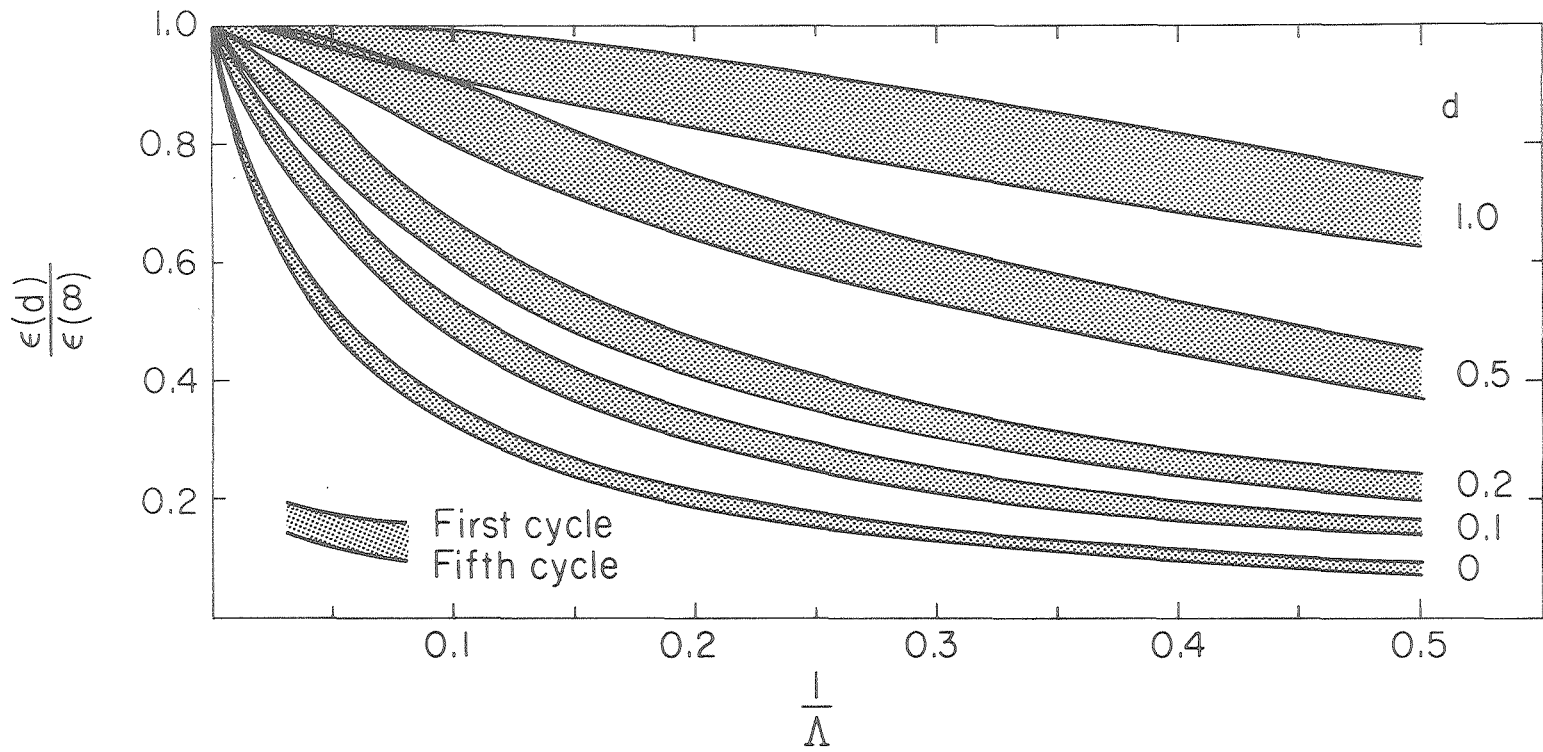


XBL8012-6591

24. Finite thickness caprock effect for the first and fifth cycle, recovery factors for $\lambda_a / \lambda_c = 1, 2, \text{ and } 10$.

FINITE THICKNESS CAPROCK EFFECT ON RECOVERY FACTOR

$$\lambda_a / \lambda_c = 2$$

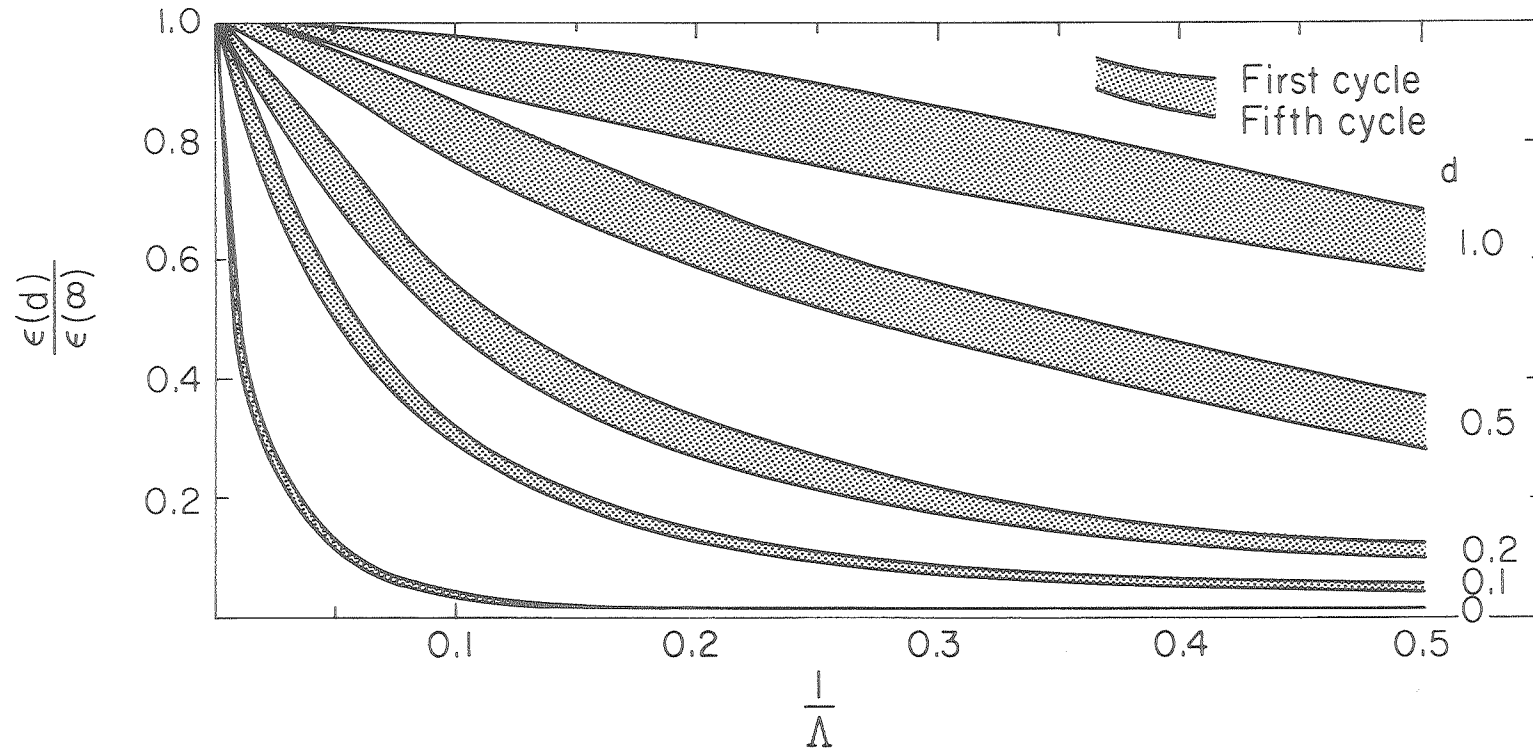


XBL8012-6592

25. Finite thickness caprock effect for the first and fifth cycle, recovery factors for $\lambda_a / \lambda_c = 1, 2, \text{ and } 10$.

FINITE THICKNESS CAPROCK EFFECT ON RECOVERY FACTOR

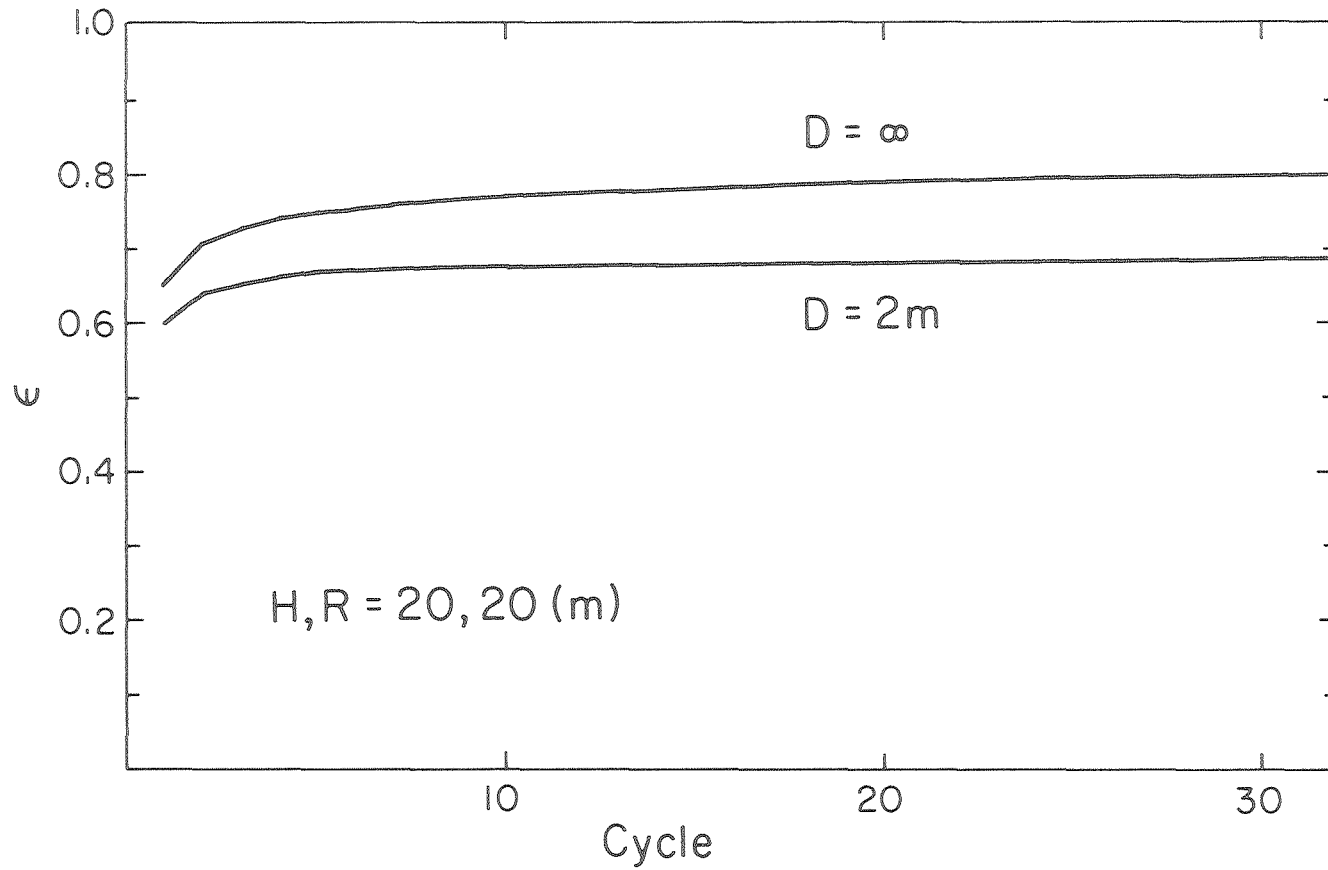
$$\lambda_a / \lambda_c = 10$$



XBL8012-6593

26. Finite thickness caprock effect for the first and fifth cycle, recovery factors for $\lambda_a / \lambda_c = 1, 2, \text{ and } 10$.

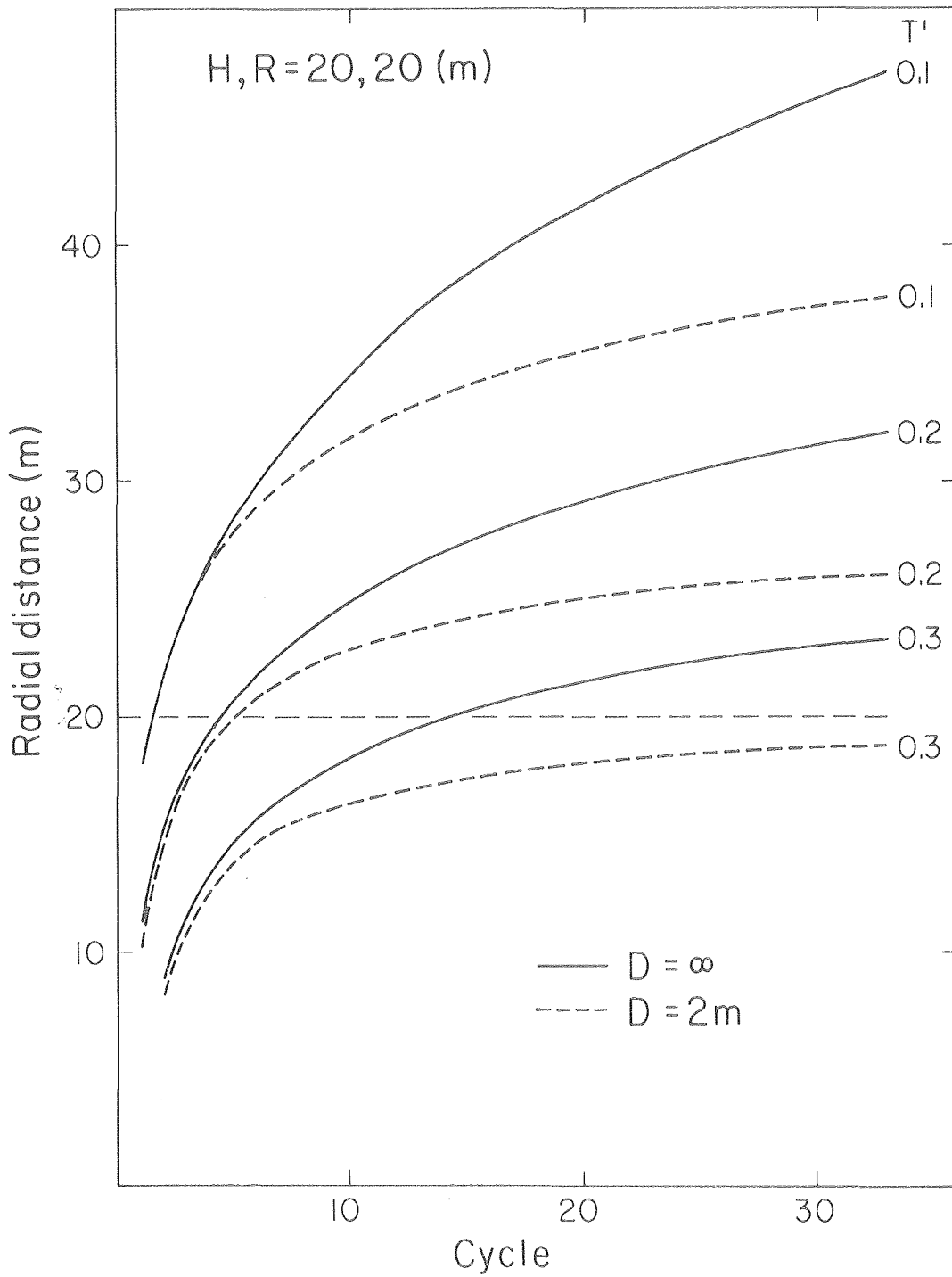
LONG TERM RECOVERY FACTOR



XBL 8012-6596

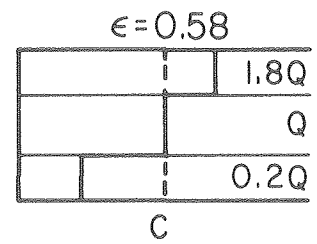
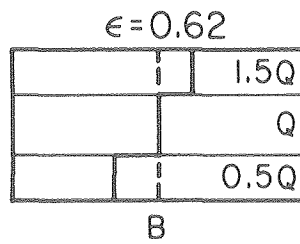
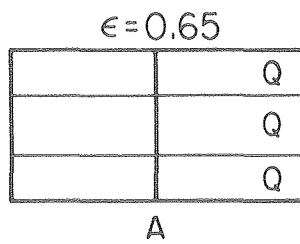
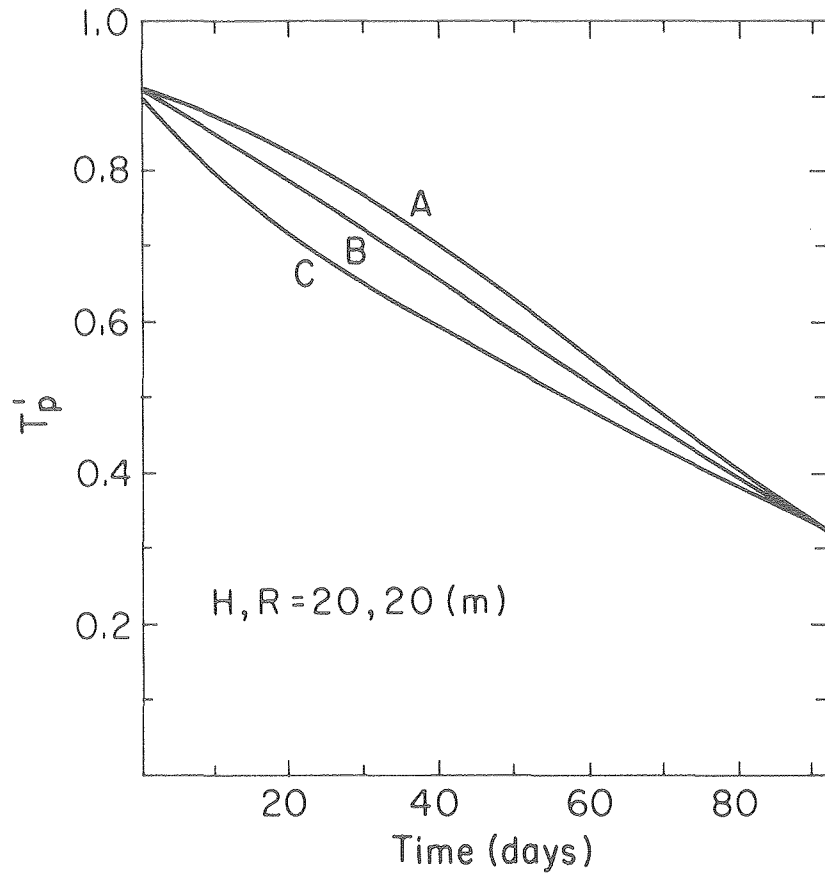
27. Recovery factor for 33 cycles for infinitely thick caprock and thin caprock cases.

LONG TERM TEMPERATURE FIELD



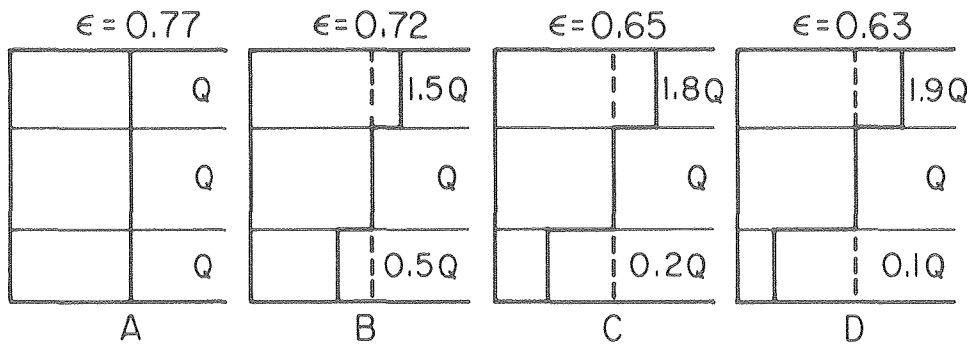
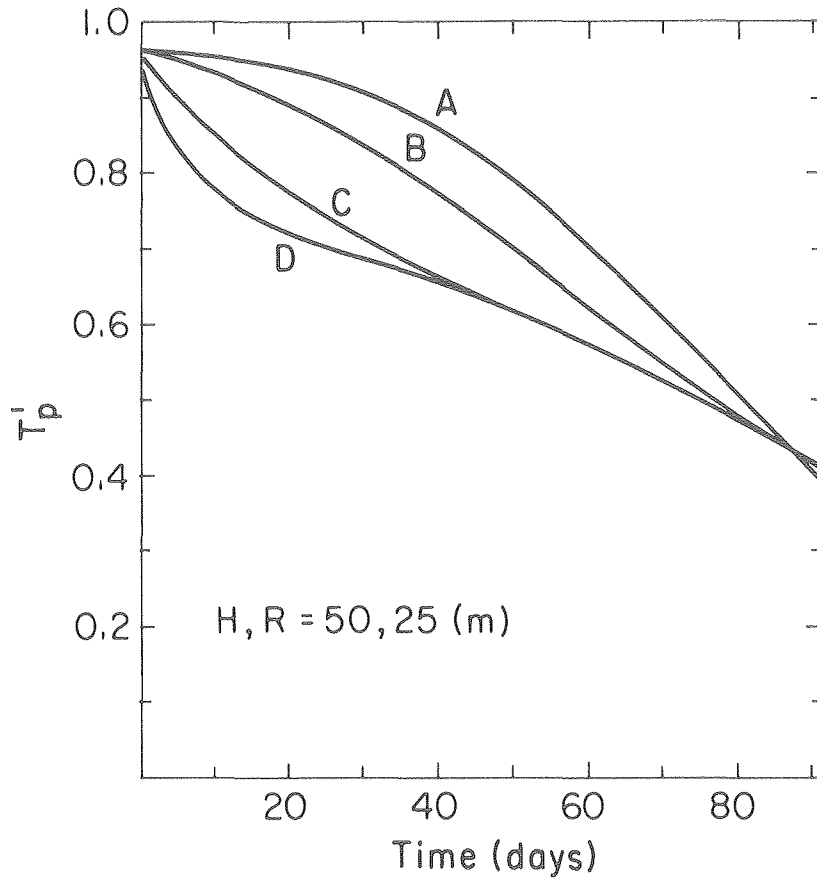
XBL8012 - 6595

28. The radial distance to several isotherms at the end of the first 33 cycles for infinitely thick caprock and thin caprock cases.



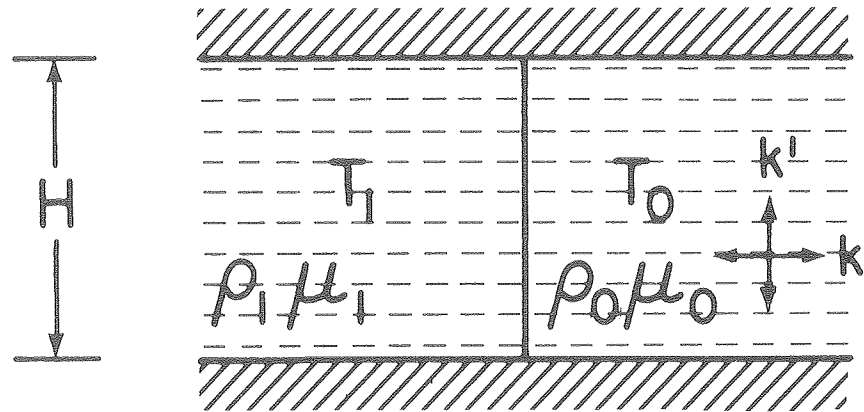
XBL 8012-6597

29. First cycle production temperature versus time for the different combination of flowrates indicated schematically in the figures, for aquifers of thickness 20 and 50 m.



XBL 8012-6598

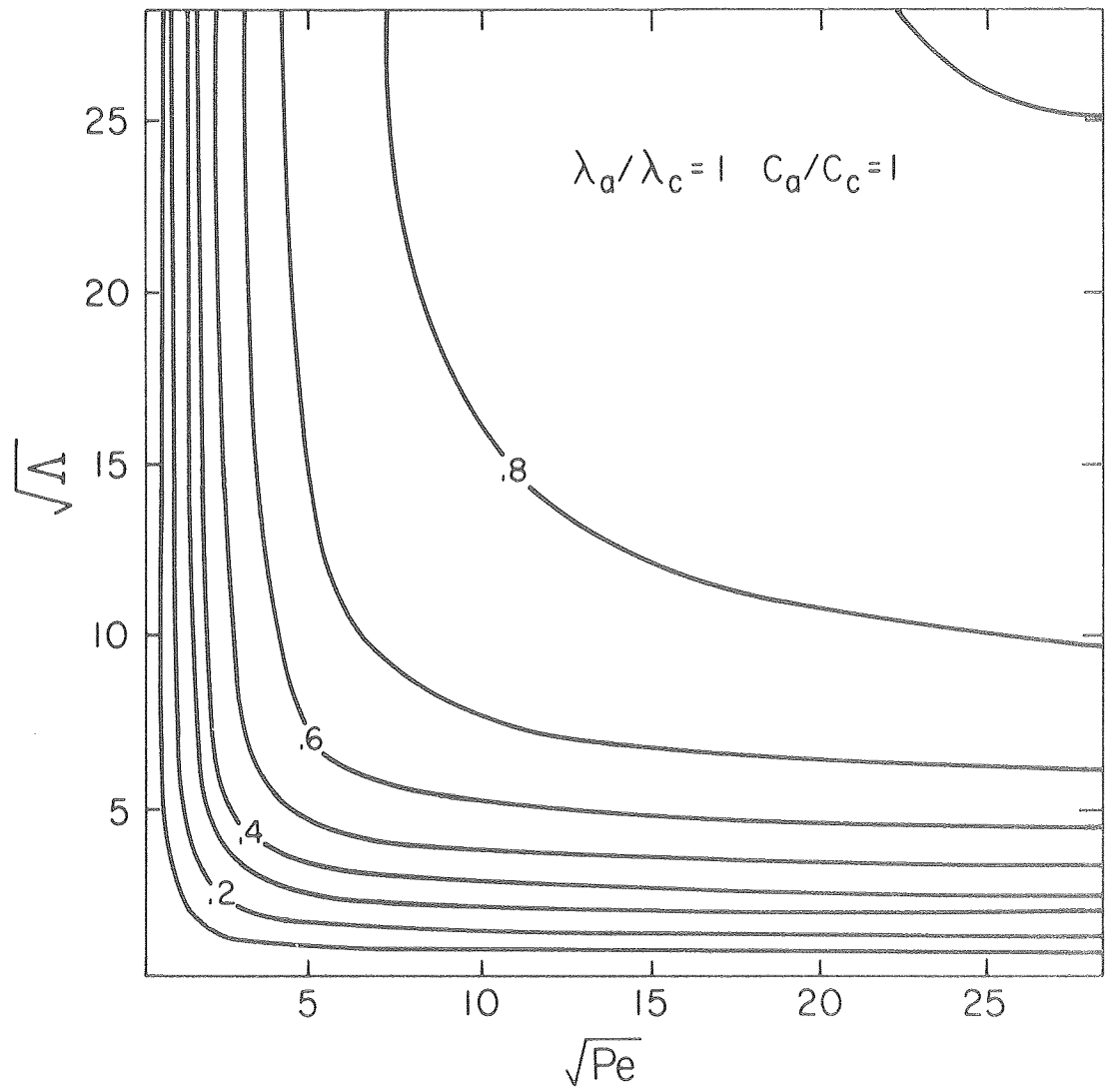
30. First cycle production temperature versus time for the different combination of flowrates indicated schematically in the figures, for aquifers of thickness 20 and 50 m.



XBL 8012-6599

A1. Schematic drawing of an aquifer with a sharp vertical thermal front.

MEAN TEMPERATURE DECLINE RECOVERY FACTOR

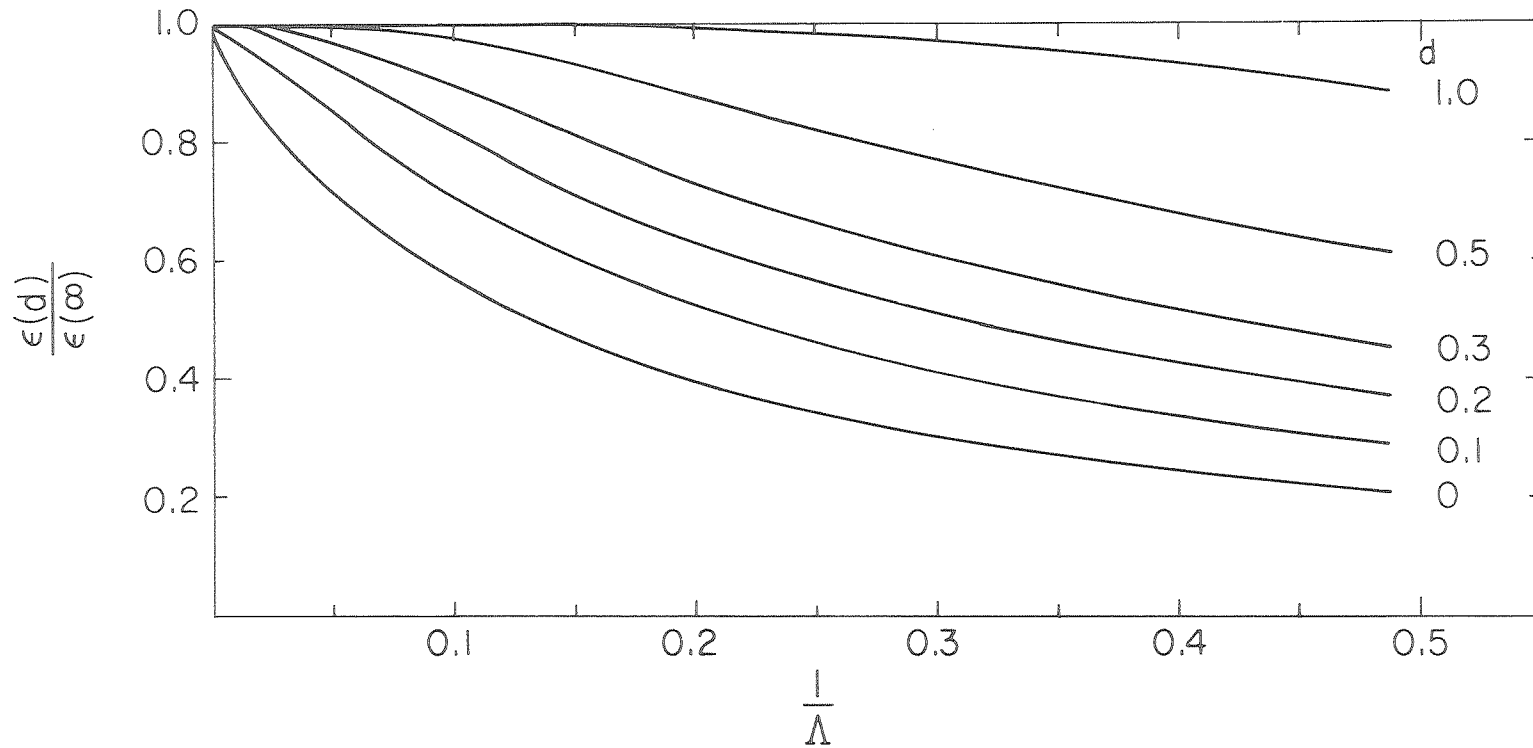


XBL 8012-6522

B1. Analytical recovery factor from the temperature decline of a cylinder.

MEAN TEMPERATURE DECLINE
FINITE THICKNESS CAPROCK EFFECT ON RECOVERY FACTOR

$$\lambda_a / \lambda_c = 1 \quad C_a / C_c = 1$$



XBL8012-6594

C1. Analytical finite thickness caprock effect on recovery factor.